

Draft version, June 14, 2019

Velocity centroids as tracers of the turbulent velocity statistics

Alejandro Esquivel and A. Lazarian

Astronomy Department, University of Wisconsin-Madison, 475 N. Charter St., Madison, WI 53706, USA

esquivel@astro.wisc.edu; lazarian@astro.wisc.edu

ABSTRACT

We use the results of magnetohydrodynamic (MHD) simulations to emulate spectroscopic observations, and produce maps of variations of velocity centroids to study their scaling properties. We compare them with those of the underlying velocity field, and analytic predictions presented in a previous paper (Lazarian & Esquivel 2003), in order to assess under which circumstances the statistical properties of the velocity field can be retrieved from velocity centroids. We tested successfully, a criteria for recovering velocity statistics from velocity centroids derived in our previous work. That is, if $\langle S^2 \rangle \gg \langle v^2 \rangle \langle I^2 \rangle$, then the structure function of a map of velocity centroids is dominated by the structure function of velocity (where S is a 2D map of “unnormalized” velocity centroids, v velocity, and I integrated intensity map or column density). We show that it is possible to extract the velocity statistics using centroids for subsonic and mildly supersonic turbulence (e. g. Mach numbers $\lesssim 2.5$). At the same time, for higher Mach number, the statistics of centroids have an important contribution arising from density fluctuations, and thus fail to trace the statistics of velocity.

Subject headings: ISM: general – ISM: structure – MHD – radio lines: ISM – turbulence

1. Introduction

It is well established that the interstellar medium (ISM) is turbulent. From the theoretical point of view, this arises from the very large Reynolds numbers found in the ISM (the Reynolds number is defined as the ratio of the dynamical timescale -or *eddy turnover time*- to the viscous damping timescale). From an observational standpoint there is also plenty of evidence that support a turbulent ISM, where the turbulence expands over scales that range from Au to kpc (Larson 1992; Armstrong, Rickett & Spangler 1995; Deshpande, Dwarakanath, & Goss 2000; Stanimirović & Lazarian 2001). This turbulence is very important for many physical processes that take place in the ISM, including star formation, cosmic ray propagation, heat transport, and heating of the ISM (for a review see Vázquez-Semadeni et al. 2000; Cho & Lazarian 2003a; and references therein).

Studies of statistics of turbulence have been fruitful using interstellar scintillations (Narayan & Goodman 1989; Spangler & Gwinn 1990). However this technique is restricted to the study of ionized media, and very importantly to density fluctuations alone (see Cordes 1999). Nowadays, radio spectroscopic observations of neutral media provides us with an enormous amount of data containing information about interstellar turbulence, including a more direct physical quantity to study turbulence: velocity. However, the emissivity of a spectral line depends on both the velocity and density fields simultaneously, and the separation of their individual contribution is not trivial. Much effort has been put into this difficult task, and several statistical measures have been proposed to extract information of velocity from spectroscopic data (see review by Lazarian 1999). Among the simplest we can mention the use of line-widths (Larson 1981, 1992; Scalo 1984, 1987). Velocity centroids have been around as measure of the velocity field for a long time now (von Hoerner 1951; Munch 1958). And they have been widely used to study turbulence in molecular clouds (Kleiner & Dickman 1985; Dickman & Kleiner 1985; Miesch & Bally 1994).

Power-spectra, correlation, and structure functions have been traditionally, and still are, the most widely used tools to characterize the statistics of emissivity maps. This statistical tools allow to study the scaling properties of turbulence, via the spectral index. Recently, more elaborated techniques have been proposed to analyze the data, such as “ Δ -variance” wavelet transform (Stutzki et al. 1998; Mc Low & Ossenkopf 2000; Ossenkopf & Mc Low 2002), or “Principal Component Analysis” (Brunt & Heyer 2002a,b; Brunt et al. 2003). These have been used with some success to extract velocity information of spectral data (mostly using maps of velocity centroids), and have some advantages, like being less sensitive to the effects of edges or noise. Regardless of the method used to examine emissivity maps, the assumption is usually that the map to analyze do trace the velocity fluctuations only. For that reason, there has been an effort in parallel to develop new statistics that trace velocity fluctuations, here we can mention the “Spectral Correlation Function” (Rosolowsky et al 1999; Padoan, Rosolowsky & Goodman 2001), “Velocity Channel Analysis” -VCA- (Lazarian & Pogosyan 2000; Lazarian et al. 2001; Esquivel et al. 2003), and “Modified Velocity Centroids” -MVCs- (Lazarian & Esquivel 2003, hereafter LE03). MVCs were derived in terms of structure functions because they allow for a fairly direct treatment of the statistics. And although in principle equivalent to correlation functions and spectra, they are known to give smaller errors in applied data analysis (see Monin & Yaglom 1975). Moreover the transformation between structure and correlation functions, or spectra is trivial. Numerical simulations provide us with an ideal testing ground for the tools available to be applied to observational data. However we must note that the situation is more complex. In one hand, real observations depend critically on the physical properties of the object under study, such as variations in the excitation state of the tracer and the radiation transfer within the cloud. As well as observing limitations: finite signal-to-noise ratio and map size, gridding effects, beam pattern, beam error, etc. On the other hand, numerical simulations have their own limitations, such as finite box size and resolution, numerical viscosity, and the physics available to a particular code. This paper is mostly concerned about the projection effects, and the impact of density fluctuations to centroid maps, which are shared by observations and simulations.

In LE03 we revised the maps of velocity centroids as a tracer of the turbulent velocity statistics, and derived analytical relations between the two point statistics of velocity centroids and the underlying velocity field. We also identified an important term which include information of density, and that can be extracted

from observables. Subtraction of that term can isolate better the velocity contribution, this yielded to a new measure that we termed “modified velocity centroids” (MVCs). In LE03 we arrived to a criterion for safe use of velocity centroids as a tool to study the scaling properties of velocity (e.g. structure functions or spectra of velocity). In this paper we present a more complete numerical study of centroids to extract turbulent velocity statistics, and include a more detailed discussion about velocity-density correlations. In §2 we review the basic problem of the density and velocity contributions to spectroscopic observations. We summarize LE03 in §3, in this paper we include two appendices with mathematical derivations omitted before due to space constraints. In §4 we test the analytical predictions, and our conclusions can be found in §5.

2. Turbulence statistics and spectral line data

In this section we pose the problem of obtaining turbulence statistics from spectral line data and establish our basic notation.

2.1. Turbulence statistics in three dimensions (xyz space).

Due to the stochastic nature of turbulence, it is convenient to use statistical tools for its description. Among such tools we have correlation and structure functions (Monin & Yaglom 1975). For instance, the two-point correlation function of a vector field, $\mathbf{u}(\mathbf{x}) = [u_x(\mathbf{x}), u_y(\mathbf{x}), u_z(\mathbf{x})]$, is defined as:

$$B_{ij}(\mathbf{r}) \equiv \langle u_i(\mathbf{x}_1) u_j(\mathbf{x}_2) \rangle, \quad (1)$$

where $\mathbf{r} = \mathbf{x}_2 - \mathbf{x}_1$ is the separation or “lag”, $i, j = x, y, z$, and $\langle \dots \rangle$ denote ensemble average over all space. An additional definition can be done in terms of the fluctuations of the field. This can be obtained formally by replacing $\mathbf{u}(\mathbf{r})$ by $\tilde{\mathbf{u}}(\mathbf{r}) = \mathbf{u}(\mathbf{r}) - \langle \mathbf{u}(\mathbf{r}) \rangle$ in equation (1). Note that this necessarily implies $\langle \tilde{\mathbf{u}} \rangle = 0$. We will refer to this variation simply as correlation function of fluctuations, and denote by

$$\tilde{B}_{ij}(\mathbf{r}) \equiv \langle \tilde{u}_i(\mathbf{x}_1) \tilde{u}_j(\mathbf{x}_2) \rangle = B_{ij}(\mathbf{r}) - \langle u_i \rangle \langle u_j \rangle. \quad (2)$$

In the same manner, it is customary to define the structure function of the same vector field $\mathbf{u}(\mathbf{x})$ as

$$\begin{aligned} D_{ij}(\mathbf{r}) &\equiv \langle [u_i(\mathbf{x}_1) - u_i(\mathbf{x}_2)] [u_j(\mathbf{x}_1) - u_j(\mathbf{x}_2)] \rangle \\ &= \langle [\tilde{u}_i(\mathbf{x}_1) - \tilde{u}_i(\mathbf{x}_2)] [\tilde{u}_j(\mathbf{x}_1) - \tilde{u}_j(\mathbf{x}_2)] \rangle. \end{aligned} \quad (3)$$

Notice that structure functions, by definition, are only function of the fluctuating part of the field and insensitive to the average value. Combining equations (1) and (3) is trivial that:

$$D_{ij}(\mathbf{r}) = 2 \left[\tilde{B}_{ij}(0) - \tilde{B}_{ij}(\mathbf{r}) \right] = 2 [B_{ij}(0) - B_{ij}(\mathbf{r})]. \quad (4)$$

Where $\tilde{B}_{ij}(0)$ is also known as the variance. The correlation of fluctuations must vanish at infinity, that is $\tilde{B}_{ij}(\mathbf{r}) \rightarrow 0$, as $r \rightarrow \infty$. Then from equation (4) is clear that $D_{ij}(\infty) = 2\tilde{B}_{ij}(0)$. Thus, if we know the structure function of a field we can obtain the structure function of fluctuations and vice versa. However, to get the correlation function from the structure function in general (as in equation [1]), we also need to know the average value of the field ($\langle \mathbf{u} \rangle$). Correlation and structure functions are equivalent in theory (aside from $\langle \mathbf{u} \rangle$). In practice, where we have a restricted averaging space, is frequent to obtain smaller errors in the determination of $D_{ij}(\mathbf{r})$ compared to $B_{ij}(\mathbf{r})$. At the same time, $\tilde{B}_{ij}(0)$ is usually better determined than $D_{ij}(\infty)$, see discussion in Monin & Yaglom (1975).

The spectral representation provides an alternate description of turbulence. The *spectral density tensor*, or *N-dimensional power-spectrum*, $F_{ij}(\mathbf{k}) = P_{ND}(\mathbf{k})$, is given through a Fourier transform of the correlation function of fluctuations:

$$F_{ij}(\mathbf{k}) = P_{ND}(\mathbf{k}) \equiv \frac{1}{(2\pi)^N} \int e^{-i\mathbf{k} \cdot \mathbf{r}} \tilde{B}_{ij}(\mathbf{r}) d^N \mathbf{r}, \quad (5)$$

where \mathbf{k} is the wave-number-vector, of amplitude $k = |\mathbf{k}| \sim 2\pi/r$, with $r = |\mathbf{r}|$, and N is the number of dimensions (i.e. P_{1D} is the one-dimensional, P_{2D} the two-dimensional, and P_{3D} the three-dimensional power spectrum). The definitions presented above are general, and also apply to scalar fields.

The power-spectrum of velocity (in the incompressible regime) has an important physical interpretation as the distribution of kinetic energy as a function of scale. If $\mathbf{u}(\mathbf{r})$ is the velocity field, the power-spectrum is the energy in scales between \mathbf{k} and $\mathbf{k} + \delta\mathbf{k}$, thus the total energy $\langle \mathbf{u}(\mathbf{r}) \rangle^2 = \int P_{ND}(\mathbf{k}) d\mathbf{k}$. Note however, that the physical interpretation is quite different if we talk about the spectra of other quantity (e.g. the power-spectra of density fluctuations).

The presence of a magnetic field introduces a preferential direction for motion. MHD turbulence gets axisymmetric in a system of reference defined by the direction of the *local* magnetic field (see reviews by Cho & Lazarian 2003a and Cho, Lazarian & Vishniac 2003). However, since the local direction changes from one place to another, this anisotropy is rather modest and it is possible to characterize the turbulence with isotropic statistics (see Esquivel et al. 2003). The use of isotropic statistics allows for substantial simplification. In this case the correlation and structure functions depend only on the magnitude of the separation (r) and not on the direction, and similarly spectra are only functions of k . For isotropic fields the correlation, structure or spectral tensors can be expressed via longitudinal (parallel to \mathbf{r} , denoted by subscript “ LL ”) or transverse (normal to \mathbf{r} , denoted by subscript “ NN ”) components (Monin & Yaglom 1975):

$$B_{ij}(r) = [B_{LL}(r) - B_{NN}(r)] \frac{r_i r_j}{r^2} + B_{NN}(r) \delta_{ij}, \quad (6a)$$

$$D_{ij}(r) = [D_{LL}(r) - D_{NN}(r)] \frac{r_i r_j}{r^2} + D_{NN}(r) \delta_{ij}, \quad (6b)$$

$$F_{ij}(k) = [F_{LL}(k) - F_{NN}(k)] \frac{k_i k_j}{k^2} + F_{NN}(k) \delta_{ij}, \quad (6c)$$

where δ_{ij} is a Kronecker delta ($\delta_{ij} = 1$ for $i = j$, and $\delta_{ij} = 0$ for $i \neq j$). Solenoidal motions (divergence free, therefore incompressible) correspond to the transverse components; whereas potential motions (curl free, compressible) correspond to the longitudinal components.

In the simplest realization of turbulence we have injection of energy at the largest scales. The energy cascades down to the small scales, at which viscous forces become important, and turbulence is dissipated. At intermediate scales, between the injection and the dissipation scales, the turbulent cascade is *self-similar*, and no particular scale can be associated. This range constitute the so called *inertial-range*, there the physical variables are proportional to simple powers of eddy sizes, and the two point statistics can be described by power-laws.

2.2. Three-dimensional power-law statistics

For power-law statistics (i.e. within the inertial range) Lazarian & Pogosyan (2000) discussed two regimes, a *short-wave-dominated* regime, corresponding to a *shallow* spectrum, and a *long-wave-dominated* spectrum, with a *steep* spectrum.

2.2.1. Steep (long-wave-dominated) spectrum

Consider an isotropic power-law energy spectrum (one dimensional power-spectrum) of the form

$$E(k) = C k^{\gamma_{1D}}. \quad (7)$$

A *steep* spectrum corresponds to spectral indices $\gamma_{1D} < -1$. The structure function can be written in terms of the energy spectrum as

$$D(r) = 2 \int_0^\infty [1 - \cos(k r)] E(k) dk. \quad (8)$$

For a power-law steep power spectrum (replacing eq.[7] into eq.[8]), the structure function also follows a power-law:

$$D(r) = A r^\nu = A r^{-1-\gamma_{1D}} \quad 0 < \nu < 2, \quad (9)$$

where $A = C\pi/[\Gamma(1 + \gamma) \sin(\pi\gamma/2)]$, and $\Gamma(x)$ is the Euler Gamma function. The relation between the spectral index of the structure function and power spectrum (or energy spectrum) can be generalized for isotropic fields to $P_{ND} \propto k^{\gamma_{ND}}$, with

$$\gamma_{ND} = -\nu - N. \quad (10)$$

For instance, the velocity (v) in Kolmogorov turbulence scales as $v \propto r^{1/3}$, which corresponds to a spectral index for the structure function of $\nu = 2/3$, to a three-dimensional power-spectrum index $\gamma_{3D} = -11/3$, a two-dimensional power-spectrum index $\gamma_{2D} = -8/3$, and a one-dimensional power-spectrum index $\gamma_{1D} = -5/3$. Note that Kolmogorov fails into the steep spectrum category.

Structure functions of the form in equation (9) are well defined only for $\nu > 0$, to satisfy $D(0) = 0$, and $\nu < 2$, so that equation representation in terms of Fourier integrals is possible (see Monin & Yaglom 1975). In this regime (see eq.[4]), the correlation functions are maximal, and finite, at $r = 0$. It is important to notice also, that in this regime, the power spectrum and the structure function are both a power-law,

but the correlation function is not (see eq. [4]). The correlation function in this case is a constant minus a growing (positive index) power-law, therefore is flat at small scales, and drops at large scales.

To illustrate the relation between the two point statistics and power-law spectra we produced three dimensional Gaussian cubes, with a prescribed (3D) spectral index of $\gamma_{3D} = -11/3$, as described in Esquivel et al. (2003). This data cubes are somewhat similar to the fractional Brownian motion fields used by Brunt & Heyer (2002a); Miville-Deschénes, Levrier & Falgarone (2003), or the *dephased* fields used in Brunt et al. (2003). We calculated the three dimensional power spectrum using Fast Fourier Transform (FFT). And calculated directly the structure function in 3D, then with the use of equation (4) we computed the correlation function (also in 3D).

For a 3D field of the size used here (216^3), averaging over all \mathbf{x} space to obtain the structure function is computationally too expensive. For that reason we restrict our average to all the combinations of lags (\mathbf{r}), calculated only on a grid of equally distant points (28 along each x, y, z direction) covering uniformly all the cube.

In Figure 1, we show the calculated 3D power spectra (averaged in k), structure and correlation functions of these Gaussian cubes (r averaged), and compare them with the prescribed scaling properties. We see a fair agreement with the power spectra and the structure functions functions.

The power spectrum in Figure 1 is not a perfect power-law, and has departures larger at small wave numbers. This is because we only have one realization (see Esquivel et al. 2003). This departure of the spectrum from power-law is evident for the structure function in Fig. 1 at small scales. The difference from the computed and prescribed correlation functions, although more evident at large separations, is also result of poor statistics at large wave-numbers. We computed the correlation function of fluctuations by subtracting the structure function from the variance (see eq[4]). The variance is determined by statistics at large small separations (large values of k), but in magnitude is on the order of the structure function at the largest scales. A relative small error (due to simple statistical fluctuations) in the ideal matching between the variance and structure functions ($D(L) \rightarrow 2B(0)$) translates in an additive error that propagates in uniform magnitude over all scales. In a linear plot, this would be only a error in the offset, but in a log-log plot this error is more evident, at large scales. To show this effect we include error bars when this error is as small as 10%.

2.2.2. Shallow (short-wave-dominated) spectrum

When the energy spectrum is shallow (i.e. $\gamma_{1D} > -1$), the fluctuations of the field are dominated by small-scales, therefore termed *short-wave-dominated* regime. In this case, neither the structure, nor correlation functions can be strictly represented by power-laws. In fact, in order for the Fourier Transforms to converge in this case, we need to introduce a critical scale r_c , such that the power spectrum is only a power-law for wave numbers corresponding to scales smaller than r_c . That is, for $r \ll r_c$, or equivalently

$k \gg k_0$, where $k_0 = 2\pi/r_c$. In other words

$$E(k) = C' \left(\frac{1}{r_c^2} + k^2 \right)^{\gamma_{1D}/2} = C' \left(\frac{1}{r_c^2} + k^2 \right)^{(-\alpha-1)/2}. \quad (11)$$

To a power spectrum of this form corresponds a structure function of fluctuations

$$\tilde{B}(r) = A' \left(\frac{r}{r_c} \right)^{\alpha/2} K_{\alpha/2} \left(\frac{r}{r_c} \right), \quad (12)$$

where $K_\alpha(x)$ is the α -order, modified Bessel function of the second kind (also sometimes referred as hyperbolic Bessel function), and $A' = C' \sqrt{\pi} / [2^{\alpha/2-1} \Gamma[(\alpha+1)/2] r_c^{-\alpha}]$. The Nth-dimensional power spectrum index for a structure function of the form $B \propto (r/r_c)^{\alpha/2} K_{\alpha/2}(r/r_c)$ can be generalized to $P_{ND} \propto (r_c^{-2} + k^2)^{\gamma_{ND}/2}$, with

$$\gamma_{ND} = -N - \alpha. \quad (13)$$

This relation is very similar to that for the long wave dominated case (eq[10]). In fact for $r \ll r_c$ the $K_{\alpha/2}$ can be expanded as $\sim (r/r_c)^{\alpha/2}$, thus the 3D correlation function (as opposed to the structure function as in the long wave dominated regime) goes as a power-law $\tilde{B}(r) \sim (r/r_c)^\alpha$ at small separations. Notice that for a shallow spectrum the structure function grows rapidly at the smallest scales and then flattens. Similarly to the steep spectrum, we produce a short-wave-dominated Gaussian 3D field, with a prescribed index of $\gamma_{3D} = -2.5$ (shallow). In Figure 2 we present the expected and calculated two point statistics. Here the critical scale r_c is determined by the smallest wave number, given by the size of the computational box ($r_c = L$).

2.3. Turbulence statistics as observed (position-position-velocity space)

In spectroscopic observations we can not observe the distribution of gas in real space ($\mathbf{x} \equiv [x, y, z]$) coordinates. Instead we observe the intensity of emission of a given spectral line at a position \mathbf{X} in the sky, and at a given velocity v along the line of sight (LOS). To distinguish 2D vectors from 3D vectors, we will use capital letters to denote the former, and lower case for the latter. Observational data are usually arranged in matrices with coordinates (\mathbf{X}, v) , also called position-position-velocity (or simply PPV) cubes. We will identify the LOS with the coordinate z . Thus, in the plane parallel approximation, the relation between real space and PPV space is that of a map $(\mathbf{X}, z) \rightarrow (\mathbf{X}, v)$, with $\mathbf{X} = (x, y)$.

At any point, the LOS velocity can be decomposed in a regular flow, a thermal and a turbulent components $[v_z(\mathbf{x}) = v_{z,reg}(\mathbf{x}) + v_{thermal} + v_{z,turb}(\mathbf{x})]$. This way, the distribution of the Doppler shifted atoms follows is a Maxwellian of the form:

$$\phi(\mathbf{x}) dv_z = \frac{1}{(2\pi\beta)^{1/2}} \exp \left\{ \frac{[v_z - v_{z,reg}(\mathbf{x}) - v_{turb,z}(\mathbf{x})]^2}{2\beta} \right\} dv_z, \quad (14)$$

where $\beta = \kappa_B T / m$, κ_B is the Maxwell-Boltzmann constant, T the temperature, and m the atomic mass. In PPV space, the density of emitters $\rho_s(\mathbf{X}, v_z)$ can be obtained integrating along the LOS

$$\rho_s(\mathbf{X}, v_z) d\mathbf{X} dv_z = \left[\int dz \rho(\mathbf{x}) \phi(\mathbf{x}) \right] d\mathbf{X} dv_z, \quad (15)$$

where $\rho(\mathbf{x})$ is the mass density of the gas in spatial coordinates. The density of emitters $\rho_s(\mathbf{X}, v_z)$ can be identified as the column density per velocity interval, commonly referred as dN/dv . Equation (15) simply counts the number of atoms at a position in the plane of the sky \mathbf{X} , with a z component of velocity in the range $[v_z, v_z + dv_z]$, and the limits of integration are defined by the LOS extent.

In what follows, we will assume that the emissivity of our media is proportional to the first power of the density (this is true for instance in the case of H I). We will consider an isothermal media, and neglect the effects of self-absorption. In this case, the integrated intensity of the emission (integrated along the velocity coordinate) is proportional to the column density:

$$I(\mathbf{X}) \equiv \int \alpha \rho_s(\mathbf{X}, v_z) dv_z = \int \alpha \rho(\mathbf{x}) dz, \quad (16)$$

where α is a constant. This assumption is satisfied for observational data where the media is optically thin, thermalized, and with constant excitation conditions. However, for any observed map the applicability of this assumption has to be examined, even for H I widespread self-absorption has now been detected (for example Jackson et al. 2002; Li & Goldsmith 2003).

The statistics available from spectral line data are spectra, correlation and structure functions in PPV space. Relations between the observable and the intrinsic 3D statistics using 2D power-spectra in channel maps was established in Lazarian & Pogosyan (2000), and tested numerically in Lazarian et al. (2001), and Esquivel et al. (2003). In LE03 we studied analytically the use of velocity centroids, to extract the underlying turbulent velocity statistics. We review this work below, and test numerically the predictions therein.

2.4. Projection of the Structure functions along the line of sight

We have seen that in spectroscopic observations we can not observe either the density or velocity fields in real space (x, y, z), but we have to deal with projections along the LOS. In Lazarian (1995) the issue of projection is discussed, in this section we briefly state some results that are relevant to this work. In Appendix A, we exemplify the projection effects discussed to the particular case of power-law statistics, and in Appendix C we carry on the algebraic steps to relate the power-spectra to the structure function of a field that has been integrated along a direction we can relate to the LOS.

Consider the structure function of the integrated intensity (column density under our assumptions of optically thin media with emissivity proportional to the first power of density) as described in equation (16):

$$\left\langle [I(\mathbf{X}_1) - I(\mathbf{X}_2)]^2 \right\rangle = \left\langle \left(\int_0^L \alpha \rho(\mathbf{x}_1) dz - \int_0^L \alpha \rho(\mathbf{x}_2) dz \right)^2 \right\rangle, \quad (17)$$

where we have written explicitly the limits of integration, with L being the size of the object (along the LOS direction). As described in (Lazarian 1995), we can expand the square in equation (17) combining the identity:

$$\left(\int \chi(x) dx \right)^2 = \iint \chi(x_1) \chi(x_2) dx_1 dx_2, \quad (18)$$

and the elementary identity

$$(a-b)(c-d) = \frac{1}{2} \left[(a-d)^2 + (b-c)^2 - (a-c)^2 - (b-d)^2 \right], \quad (19)$$

to obtain

$$\langle [I(\mathbf{X}_1) - I(\mathbf{X}_2)]^2 \rangle = \alpha^2 \int_0^L \int_0^L dz_1 dz_2 \left[d_\rho(\mathbf{r}) - d_\rho(\mathbf{r})|_{\mathbf{X}_1=\mathbf{X}_2} \right]. \quad (20)$$

Where $d_\rho(\mathbf{r})$ is the 3D structure function of the density,

$$d_\rho(\mathbf{r}) = \langle [\rho(\mathbf{x}_1) - \rho(\mathbf{x}_2)]^2 \rangle. \quad (21)$$

Notice that this definition is general, and does not require any particular functional form of the 3D structure functions (i.e. power-law statistics). The problem of formally inverting equation (20) to obtain the underlying statistics, allowing for anisotropic turbulence has been presented in Lazarian (1995). We include in Appendix A details for the special case of isotropic 3D power-law statistics. For the present work is sufficient to say that for fields which are homogeneous, isotropic, and have a power-law spectrum: the structure functions of the integrated fields (2D maps) can be approximated by power-laws at both small or large scales (see Minter 2002, and also Appendix A). For instance if the density has a power-spectrum $P_{3D,\rho} \propto k^{\gamma_{3D}}$, the structure function of column density will have the form

$$\langle [I(\mathbf{X}_1) - I(\mathbf{X}_2)]^2 \rangle \propto R^\mu, \quad (22)$$

where R is the separation in the plane of the sky ($R = |\mathbf{R}| = |\mathbf{X}_2 - \mathbf{X}_1|$), and

$$\mu \approx \begin{cases} -\gamma_{3D} - 2 & \text{for } R \ll L \text{ (for both steep or shallow spectrum),} \\ -\gamma_{3D} - 3 & \text{for } R \gg L, \text{ and } \gamma_{3D} < -3 \text{ (steep spectrum),} \\ 0 & \text{for } R \gg L, \text{ and } \gamma_{3D} > -3 \text{ (shallow spectrum).} \end{cases} \quad (23)$$

The asymptotic behavior at small scales is illustrated in Figure (3) for the Gaussian cubes used above. Where we show the computed two point statistics after integrating the cubes along the z direction.

If the LOS size of the cloud is much smaller than the size in the plane of the sky (so $R \gg L$ is possible) we see the underlying 3D statistics of the structure functions for large separations (i.e. no projection effect). Another subtle, yet interesting, point is that the power spectrum of an integrated field recovers only the solenoidal (incompressible) component of the velocity field, as we stated in LE03 (see also Appendix C). This could be potentially used to study the role of compressibility in turbulence statistics, by combining results of centroids and VCA.

3. Modified velocity centroids revisited.

Velocity centroids have been widely used to relate their statistics with velocity, their conventional form is (Miesch & Bally 1994)

$$C(\mathbf{X}) = \frac{\int v_z \rho_s(\mathbf{X}, v_z) dv_z}{\int \rho_s(\mathbf{X}, v_z) dv_z}. \quad (24)$$

We will refer to this definition as “normalized” centroids. The denominator in equation (24) introduces an extra algebraic complication for a direct analytical treatment of the two-point statistics. For the sake of simplicity we start considering “unnormalized” velocity centroids:

$$S(\mathbf{X}) = \int v_z \rho_s(\mathbf{X}, v_z) dv_z. \quad (25)$$

Similarly to the expression in equation (16), with emissivity proportional to the first power of the density, and no self absorption, the structure function of the unnormalized velocity centroids is:

$$\langle [S(\mathbf{X}_1) - S(\mathbf{X}_2)]^2 \rangle = \left\langle \left(\alpha \int v_z(\mathbf{x}_1) \rho(\mathbf{x}_1) dz - \alpha \int v_z(\mathbf{x}_2) \rho(\mathbf{x}_2) dz \right)^2 \right\rangle. \quad (26)$$

We assume that the density and velocity can be presented as a sum of a mean value and a fluctuating part: $\rho = \rho_0 + \tilde{\rho}$, $v_z = v_0 + \tilde{v}_z$; where $\rho_0 = \langle \rho \rangle$, $v_0 = \langle v_z \rangle$. And the fluctuating parts satisfy $\langle \tilde{\rho} \rangle = 0$, $\langle \tilde{v}_z \rangle = 0$. Analogously to the derivation of equation (20), the structure function of the unnormalized centroids can be written as

$$\langle [S(\mathbf{X}_1) - S(\mathbf{X}_2)]^2 \rangle = \alpha^2 \iint dz_1 dz_2 [D(\mathbf{r}) - D(\mathbf{r})|_{\mathbf{X}_1=\mathbf{X}_2}], \quad (27)$$

with

$$D(\mathbf{r}) = \left\langle [v_z(\mathbf{x}_1) \rho(\mathbf{x}_1) - v_z(\mathbf{x}_2) \rho(\mathbf{x}_2)]^2 \right\rangle. \quad (28)$$

And $D(\mathbf{r})$ can be approximated as:

$$D(\mathbf{r}) \approx \langle v_z^2 \rangle d_\rho(\mathbf{r}) + \langle \rho^2 \rangle d_{v_z}(\mathbf{r}) - \frac{1}{2} d_\rho(\mathbf{r}) d_{v_z}(\mathbf{r}) + c(\mathbf{r}), \quad (29)$$

which includes the underlying 3D structure of the LOS velocity

$$d_{v_z}(\mathbf{r}) = \left\langle [v_z(\mathbf{x}_1) - v_z(\mathbf{x}_2)]^2 \right\rangle \quad (30)$$

and $c(\mathbf{r})$ are the terms with cross-correlations of velocity and density fluctuations¹:

$$c(\mathbf{r}) = 2 \langle \tilde{v}_z(\mathbf{x}_1) \tilde{\rho}(\mathbf{x}_2) \rangle^2 + 4\rho_0 \langle \tilde{\rho}(\mathbf{x}_1) \tilde{v}_z^2(\mathbf{x}_1) \rangle - 4\rho_0 \langle \tilde{\rho}(\mathbf{x}_1) \tilde{v}_z(\mathbf{x}_1) \tilde{v}_z(\mathbf{x}_2) \rangle. \quad (31)$$

¹Note that equation (31) is somewhat different from LE03, where there was a misprint; which has no effect on the results presented.

Because the derivation of equations (27), (29), and (31) involves some tedious algebra, we include it in Appendix B. Using equations (27), (29), and (31) we can also decompose the structure function of unnormalized velocity centroids as

$$\langle [S(\mathbf{X}_1) - S(\mathbf{X}_2)]^2 \rangle = I1(\mathbf{R}) + I2(\mathbf{R}) + I3(\mathbf{R}), \quad (32)$$

where

$$I1(\mathbf{R}) = \alpha^2 \langle v_z^2 \rangle \iint dz_1 dz_2 \left[d_\rho(\mathbf{r}) - d_\rho(\mathbf{r})|_{\mathbf{X}_1=\mathbf{X}_2} \right], \quad (33a)$$

$$I2(\mathbf{R}) = \alpha^2 \langle \rho^2 \rangle \iint dz_1 dz_2 \left[d_{v_z}(\mathbf{r}) - d_{v_z}(\mathbf{r})|_{\mathbf{X}_1=\mathbf{X}_2} \right], \quad (33b)$$

$$\begin{aligned} I3(\mathbf{R}) = \alpha^2 \iint dz_1 dz_2 & \left[-\frac{1}{2} d_\rho(\mathbf{r}) d_{v_z}(\mathbf{r}) + \frac{1}{2} d_\rho(\mathbf{r})|_{\mathbf{X}_1=\mathbf{X}_2} d_{v_z}(\mathbf{r})|_{\mathbf{X}_1=\mathbf{X}_2} \right. \\ & \left. + c(\mathbf{r}) - c(\mathbf{r})|_{\mathbf{X}_1=\mathbf{X}_2} \right]. \end{aligned} \quad (33c)$$

With this new decomposition is more evident the definition of the structure function of “modified” velocity centroids (MVCs), which is

$$\begin{aligned} M(\mathbf{R}) &= I2(\mathbf{R}) + I3(\mathbf{R}) \\ &= \langle [S(\mathbf{X}_1) - S(\mathbf{X}_2)]^2 \rangle - I1(\mathbf{R}) \\ &= \langle [S(\mathbf{X}_1) - S(\mathbf{X}_2)]^2 - \langle v_z^2 \rangle [I(\mathbf{X}_1) - I(\mathbf{X}_2)]^2 \rangle. \end{aligned} \quad (34)$$

The velocity dispersion $\langle v_z^2 \rangle$ can be obtained observationally from the second moment of the spectral lines

$$\langle v_z^2 \rangle \equiv \frac{\int v_z^2 \rho_s(\mathbf{X}, v_z) dv_z}{\int \rho_s(\mathbf{X}, v_z) dv_z}, \quad (35)$$

and $\langle [I(\mathbf{X}_1) - I(\mathbf{X}_2)]^2 \rangle = \langle v_z^2 \rangle^{-1} I2(\mathbf{R})$ is the structure function of the column density (see Lazarian 1995). In terms of the intrinsic velocity and density statistics equation (34) becomes

$$\begin{aligned} M(\mathbf{R}) \approx & \alpha \langle v_z^2 \rangle \langle \rho^2 \rangle \iint dz_1 dz_2 \{ [b(\mathbf{r}) + c(\mathbf{r})] \\ & - [b(\mathbf{r})|_{\mathbf{X}_1=\mathbf{X}_2} + c(\mathbf{r})|_{\mathbf{X}_1=\mathbf{X}_2}] \}, \end{aligned} \quad (36)$$

with

$$b(\mathbf{r}) = \frac{d_{v_z}(\mathbf{r})}{\langle v_z^2 \rangle} \left(1 - \frac{1}{2} \frac{d_\rho(\mathbf{r})}{\langle \rho^2 \rangle} \right). \quad (37)$$

The contribution of velocity-density cross-correlations ($c[\mathbf{r}]$) have been studied earlier. For VCA it has been shown that is marginal (Lazarian et al. 2001; Esquivel et al. 2003). However, subtracting the main contribution of the density fluctuations increases the relative importance of the cross terms. Therefore a more detailed discussion in the context of MVCs is necessary, this can be found below.

If $I2(\mathbf{R}) \gg I3(\mathbf{R})$, we are left with a map of integrated turbulent velocity. And we can recover the underlying 3D velocity statistics from the MVCs. To show this, take a two dimensional Fourier transform of the resulting structure function of modified velocity centroids,

$$P_{2D}(\mathbf{K}) = \frac{1}{4\pi^2} \int d^2\mathbf{R} e^{-i\mathbf{K}\cdot\mathbf{R}} I2(\mathbf{R}). \quad (38)$$

Combining equations (6a), (33b), (38), and some algebra presented in Appendix C one gets:

$$P_{2D}(K) = C_1 F_{NN}(K, 0) + C_2 \delta(K). \quad (39)$$

Where C_1, C_2 are constants. We should note that we only obtain the statistics of the solenoidal component of the velocity. But, if the turbulent velocity field is mostly solenoidal, as supported by numerical simulations (Matthaeus et al. 1996; Porter, Woodward & Pouquet 1998; Cho & Lazarian 2003b), the power-spectrum is uniquely defined assuming isotropy ($E(k) \approx 4\pi k^2 F_{NN}(k)$).

With this background we arrived in LE03 to a criterion for safe use of velocity centroids: *if $\langle S^2 \rangle \gg \langle v_z^2 \rangle \langle I^2 \rangle$ then the velocity centroids structure function ($\langle [S(\mathbf{X}_1) - S(\mathbf{X}_2)]^2 \rangle$) will mostly trace the turbulent velocity statistics, otherwise the density fluctuations are important and will be reflected in the centroid measures.* However, if the cross terms can be neglected, one could in principle subtract the contribution of density and the MVCs would trace the velocity statistics. The criteria had the implicit assumption that $I2(\mathbf{R}) \gg I3(\mathbf{R})$, at the scales of our interest.

A natural question arises: how large is the magnitude $I3(\mathbf{R})$ compared to the rest of the terms in equation (32)? First of all we should observe that $\langle [S(\mathbf{X}_1) - S(\mathbf{X}_2)]^2 \rangle$ is positive defined, and so are $I1(\mathbf{R})$ and $I2(\mathbf{R})$. Therefore to keep $\langle [S(\mathbf{X}_1) - S(\mathbf{X}_2)]^2 \rangle$ positive, $I3(\mathbf{R})$ must always be smaller than the sum of $I1(\mathbf{R})$ and $I2(\mathbf{R})$. To go deeper, let start noting that $I3(\mathbf{R})$ consist in a sum of two contributions. The first being a product of the density and LOS velocity structure functions, and the second arising from cross-correlations of velocity and density (grouped in what we called $c[\mathbf{r}]$). For the moment, we will focus on the contribution from the integrals of the product of the density and LOS velocity structure functions, and we will also refer to it simply as “cross term” (neglecting $c(\mathbf{r})$, which we shall refer to as “cross-correlations” of ρ and v_z). The cross term is maximal at large scales, and so are $I1(\mathbf{R})$ and $I2(\mathbf{R})$. At the largest scale $d_\rho(L) \rightarrow 2\langle \tilde{\rho}^2 \rangle$, $d_{v_z}(L) \rightarrow 2\langle \tilde{v}_z^2 \rangle$, and at this particular scale $I3(\mathbf{R})$ is on the order of the sum of $I1(\mathbf{R})$ and $I2(\mathbf{R})$. Although in $I2(\mathbf{R})$, the structure function of velocity is weighted by $\langle \rho^2 \rangle$ instead of only $\langle \tilde{\rho}^2 \rangle$, which enhance the velocity statistics compared to the cross term. The importance of the cross term at the smaller scales (in which we are most interested, because is where one have better statistics) will depend on how steep the underlying structure functions are.

To better understand this, consider a particular case of steep power-law statistics of the form $d_\rho(r) \propto r^n$, and $d_{v_z}(r) \propto r^m$, with ($m, n > 0$). Here the cross term in consideration scales as $\propto r^{m+n}$, steeper than both velocity and density. Given that at large scales the sum of $I1(\mathbf{R})$ and $I2(\mathbf{R})$, is on the order of the $I3(\mathbf{R})$ and the latter falls more rapidly toward small scales (steeper), its contribution will always be smaller than both velocity and density structure functions at small scales. If the density or the LOS velocity (or both), have a shallow spectrum (structure spectral index < 0), the cross term can be larger than $I1(\mathbf{R})$,

or $I2(\mathbf{R})$ (but not the sum). In this case the contribution of $I3(\mathbf{R})$ can significantly affect the statistics of centroids. Measured spectral index of density in the literature, range from $\gamma_{3D} \sim -2.5$ to $\gamma_{3D} \sim -4.0$, which include both shallow and steep cases. This is true for observations in different environments in the ISM (for instance, Deshpande et al. 2000; Bensch, Stutzki & Ossenkopf 2001; Stanimirović & Lazarian 2001; Ossenkopf & Mc Low 2002), as well as for numerical simulations (see Cho & Lazarian 2002; Brunt & Mac Low 2004). The velocity spectral index is less known from observations but has been measured to be only in the steep regime (for example using VCA, Stanimirović & Lazarian 2001), and is also in agreement with simulations. From the theoretical standpoint, at small scales when self-gravity is important we might expect clumping that result on enhanced small scale structure (yielding a shallow spectrum). On the other hand there are no clear physical grounds to our knowledge to produce a small scale dominated (shallow) velocity field. However, even in the case of steep density and velocity spectra cross-correlations of density and velocity ($c[\mathbf{r}]$), could become important. Unfortunately, direct computation of $c(\mathbf{r})$ is computationally very expensive, and we reserve its discussion for the next section, in which we will analyze the contribution of $I3(\mathbf{R})$ as a whole.

4. Testing velocity centroids numerically

In LE03 we performed some preliminary tests of the modified velocity centroids using numerical simulations, and compared the power-spectrum with that of velocity field, normalized (equation 24), and unnormalized centroids (equation 25). In this section we provide a more detailed test to investigate under what conditions velocity centroids recover the velocity statistics.

4.1. The data

We took compressible MHD data cubes from the numerical simulations of Cho & Lazarian (2003b). This data cubes correspond to fully-developed (driven) turbulence. The turbulence is driven in Fourier Space (solenoidal) at wave-numbers $2 \geq k_{driving} < 3.4$, where k is in units of $2\pi L/\lambda$ (i.e. $k = 1$ corresponds to a wave-length $\lambda = 2\pi$, λ in units of the box size L). The data cubes have a resolution of 216^3 pixels. We use four sets of simulations, and the parameters for each run are summarized in Table 1. The parameters for all the runs presented can be found in the ISM under different situations. For more details about the simulations, we refer the reader to Cho & Lazarian (2003b). The outcome of the simulations is density and velocity data cubes, which we use to create the centroids. In this paper we do not modify the spectral index of the simulations leaving intact the existing correlations between density and velocity fields, which are consistent with MHD evolution.

4.2. Results from MHD simulations

To analyze data using velocity centroids we only need with a few 2D maps, and is possible to use directly correlation or structure functions, instead of only power-spectra, both give equivalent information. The latter is less computationally intensive because FFT can be used, however for observational data at the expense of loosing precision due to periodicity issues (see Bensch et al. 2001). In fact, because the large number of channels in the case of the VCA we were restricted to use exclusively power-spectra. Despite the fact that the simulations presented in this paper are obtained with periodic boundary conditions, we will use mostly structure functions. This, because the analytical treatment is more direct than using spectra, and can be easily translated to correlation functions or spectra. We should notice anyway, that from radio interferometric observations (see Lazarian 1995) spectrum can be obtained directly. In contrast to the 3D structure functions calculated in §2, where we performed the average over all possible values of the lag (\mathbf{r}) but only on a restricted subset of the possible positions in the data cube (\mathbf{x}). For the structure functions of integrated quantities (2D) we did the average also over all spatial positions (\mathbf{x}).

Before we study the 2D maps and try to extract from those the underlying (3D) statistics, and since from the numerical simulations we have direct access to them; we will start by computing the power spectra and structure functions in 3D. This is presented in Figure 4. It is noticeable that only for the case where the turbulence is subsonic (uppermost panel in Figure 4) the amplitude of the velocity fluctuations is larger than that of the density fluctuations. Spectral indices, both for spectra and structure functions in Figure 4 are given in Table 2. The indices for power-spectra were obtained for a range in wave number $k \sim 5 - 22$ (between the scale of injection and the scales at which dissipation is dominant), for the structure functions we used the corresponding values for spatial separations ($r \sim L/5 - L/22$). Power spectra for the density becomes shallow for larger Mach numbers. At the same time spectral index of velocity changes to steeper values, but in less proportion compared to the density.

A natural way to start studying how the velocity centroids trace the statistics of velocity is to compare their structure function with that of a map of the integrated velocity:

$$\left\langle [V_z(\mathbf{X}_1) - V_z(\mathbf{X}_2)]^2 \right\rangle = \left\langle \left[\int v_z(\mathbf{x}_1) dz - \int v_z(\mathbf{x}_2) dz \right]^2 \right\rangle. \quad (40)$$

This map of integrated velocity can be used to obtain the velocity statistics in the same way that column density can be used to obtain the statistics of density. Therefore it is a direct measure of the underlying velocity statistics (see Appendix C). However, is not observable, while velocity centroids are. We computed the structure functions of 2D maps of the various centroids (normalized, unnormalized, and “modified”) and integrated velocity. The results are presented in Figure 5. To allow for a fair comparison between the different quantities plotted, we normalized them to units of $[v_z^2 \rho^2]$. That is, we multiplied the structure function of the integrated velocity by $\langle \rho^2 \rangle$, the integrated density by $\langle v_z^2 \rangle$, and the normalized centroids by $\langle I^2 \rangle$. We also present in Table 3 a summary of spectral indices (slope in the log-log plot) measured from Figure 5. Due to the finite width effects discussed at the end of section 2.4, to obtain the spectral index from the structure functions presented in Figure 5 we should restrict ourselves to measure the log-log-slope for the smallest separations. However such scales are already dominated by dissipation. For that reason is difficult

to provide a quantitative measure for the spectral index for the integrated quantities. However a comparative measure between the spectral index of centroids to that of integrated velocity or density is possible. We computed the spectral indices reported in Table 3 using wave-numbers only between ~ 5 , and ~ 22 . This problem may be alleviated for real observations were we have a larger inertial range (provided that the spatial resolution is enough to have, say over two decades of spatial range -in \mathbf{X} - bellow the LOS size of the cloud). From the figure we can immediately see that the relative importance of the density and velocity statistics on the centroids depend on the strength of the turbulence (i.e. on the Mach number), as expected from our explicit calculation of the 3D two point statistics. In the first panel (*a*), the Mach number is low, the level of the density fluctuations is very small compared to the velocity fluctuations (weighted by $\langle v_z^2 \rangle$ and $\langle \rho^2 \rangle$ respectively), and all the centroids trace very well the underlying velocity statistics. Also, in this case the criteria $\langle S^2 \rangle / (\langle v_z^2 \rangle \langle \rho^2 \rangle) \gg 1$ is well satisfied. For the rest of the cases (*b*, *c*, and *d*) the density has an increasing impact which is reflected in the centroids, and the criteria is not strictly met. The result presented in Figure 5(*a*) also agrees with the common knowledge that velocity centroids trace turbulent velocity statistics in the case of subsonic turbulence (i.e. where density fluctuations are expected to be negligible, almost incompressible). In our simulations, we notice however, that velocity centroids recover the scaling properties of the turbulent velocity field even if the turbulence is supersonic, at least for Mach numbers $\lesssim 2.5$ (Fig. 5[*b,c*]). This in despite of the criteria is not very well satisfied, $\langle S^2 \rangle / (\langle v_z^2 \rangle \langle \rho^2 \rangle) \approx 4.6$, 4.4 respectively. These two cases are in the borderline, the criteria is not strictly satisfied, and there is indeed an important contribution of the density fluctuations. But still the structure function of velocity dominates the centroids statistics. Also, in this cases we also see a slight improvement on the MVCs compared to the other two centroids. For strongly supersonic turbulence, as illustrated in Figure 5(*d*), centroids do not reflect the statistics of velocity, and the criteria is not fulfilled ($\langle S^2 \rangle / (\langle v_z^2 \rangle \langle \rho^2 \rangle) \approx 2.2$). This is consistent with the results presented in LE03 were we see evidence of a density dominated regime at small scales (see also Brunt & Mac Low 2004). We should note that although MVCs show some improvement over the other two type of centroids, subtracting two functions that are plotted in a log-log scale introduce substantial errors in the spectral index, especially if the term subtracted has a shallow spectrum. This is because to a shallow spectrum corresponds a structure function that flattens at large separations, and the effect of subtracting it is similar to that discussed at the end of section 2.2.1.

The remaining $I3(\mathbf{R})$ term has contributions of velocity and density that we can not disentangle. To study its importance, we plot $\langle [S(\mathbf{X}_1) - S(\mathbf{X})]^2 \rangle$, as decomposed in equation (32), in Figure 6. We do not calculate explicitly $I3(\mathbf{R})$ because is computationally prohibiting, but we estimate the residual of subtracting $I1(\mathbf{R}) + I2(\mathbf{R})$ from the structure function of the centroids map (in fact, because $I3(\mathbf{R})$ has negative terms, we computed $|\langle [S(\mathbf{X}_1) - S(\mathbf{X})]^2 \rangle - I1(\mathbf{R}) - I2(\mathbf{R})|$). Our results suggest that for low Mach numbers $I3(\mathbf{R})$ (the cross term and cross-correlations) can be safely neglected if compared to the contribution of the velocity structure function term ($I2([\mathbf{R}])$), but their relative importance becomes larger as the strength of turbulence increases. For Mach numbers $\lesssim 2.5$ the velocity centroids statistics are still dominated by velocity. While for our case of strongest turbulence neither $\langle S^2 \rangle \gg \langle v_z^2 \rangle \langle I^2 \rangle$, nor $I2(\mathbf{R}) \gg I3(\mathbf{R})$ are satisfied. And therefore is not surprise that all the kind of centroids used here fail in tracing the scaling of turbulent velocity. At this point it is not clear whether $I3(\mathbf{R})$ becomes important because the density spectrum of density or high cross correlations. But certainly, as the turbulence becomes more

supersonic one should expect an increase of the “cross-term” (product of velocity correlations and density correlations) as well as density-velocity cross-correlations.

For the cases where the criteria is marginally fulfilled at a first glance it might seem surprising that the velocity centroids are dominated by velocity even when the 3D structure functions of density had a zero point larger than that of velocity. This effect arises primarily from the fact that the density is positive defined, and necessarily has a non zero mean, whereas the velocity field can (and we want it to) have a zero mean. This can be seen from the factors that multiply the density and velocity structure functions in equation (29). The factor $\langle v_z^2 \rangle = v_0^2 + \langle \tilde{v}_z^2 \rangle$ multiplies the density structure function, and we can minimize the undesired density contribution by shifting our velocity axis in such a way that $v_0 = 0$.

5. Summary and conclusions

We used MHD data cubes to produce centroid maps, and showed that velocity centroids are a valuable tool to study the turbulent velocity scaling properties from spectral line data.

We investigated numerically the analytical predictions in our previous study of velocity centroids (LE03). In particular, we tested successfully the criteria for which velocity centroids give trustworthy information. That is, $\langle S^2 \rangle / (\langle v_z^2 \rangle \langle I^2 \rangle) \gg 1$. Where $\langle S^2 \rangle$ is the variance of the *unnormalized* velocity centroids (defined in eq.[25]) 2D map, $\langle v_z^2 \rangle$ the velocity dispersion (attainable through the second moment of the spectral lines), and $\langle \rho^2 \rangle$ the variance of the map of column density. We should stress that this criteria is defined in terms of a variation of the velocity centroids (unnormalized), instead of the usual definition (which we term *normalized*). For our data cubes, we found that when the criteria is fulfilled ($\langle S^2 \rangle / (\langle v_z^2 \rangle \langle \rho^2 \rangle) \gtrsim 90$) we can recover the turbulent velocity statistics from centroids. Two cases where the criteria was barely satisfied ($\langle S^2 \rangle / (\langle v_z^2 \rangle \langle \rho^2 \rangle) \gtrsim 4$) showed signs of being affected partially by density fluctuations. However in the cases, with Mach numbers of ~ 2.5 , we found that the statistics of centroids were still dominated by velocity. This puts a practical upper limit on the strength of turbulence that can be studied using velocity centroids. Nevertheless, we must recognize that this study was done using a limited data set. A more complete exploration of parameter space is desirable to best determine the range of applicability of velocity centroids, and will certainly be done in the near future. MVC were found to trace equally or better the velocity statistics than ordinary centroids. For data cubes of strongly supersonic turbulence (Mach number ~ 7), where the criteria was not fulfilled, velocity centroids failed to trace the velocity statistics. This results are in good agreement with those presented by Brunt & Mac Low (2004).

We thank Jungyeon Cho for providing the numerical simulations used in this paper. We also thank Anthony Minter, the referee of LE03, for suggestions that resulted in an improvement of this work, and V. Ossenkopf and J. Stutzki for valuable comments. A. E. acknowledges financial support from CONACyT (Mexico). A. L. research is supported by NSF grant AST 0307869 and the NSF Center for Magnetic Self Organization in Laboratory and Astrophysical Plasmas.

A. Projection of structure functions of a power-law spectrum field

In this section we exemplify the long-wave dominated (steep) case as if coming from a velocity field, while the shallow case as if from a density field. But the results are interchangeable, depending on the specific spectral index they have (although there is no physical motivation to consider a shallow the velocity field).

A.1. Projection of a field with a steep power spectrum

Consider a homogeneous, and isotropic velocity field with a *steep* power-law spectrum. The LOS velocity structure function will be of the form:

$$\langle [v_z(\mathbf{x}_1) - v_z(\mathbf{x}_2)]^2 \rangle = C_1 r^m. \quad (\text{A1})$$

Where $r = \sqrt{R^2 + (z_2 - z_1)^2}$, R is the separation in the plane of the sky ($R^2 = [x_2 - x_1]^2 + [y_2 - y_1]^2$), and $(z_2 - z_1)$, the separation along the LOS. This way we can rewrite the 3D power-law structure function as

$$\langle [v_z(\mathbf{x}_1) - v_z(\mathbf{x}_2)]^2 \rangle = C_1 \left[R^2 + (z_2 - z_1)^2 \right]^{m/2}. \quad (\text{A2})$$

With this structure function, the projection of the velocity field, as described in §2.4 applied to this isotropic case is

$$\langle [V_z(\mathbf{X}_1) - V_z(\mathbf{X}_2)]^2 \rangle = C_1 \int_0^L \int_0^L \left\{ \left[R^2 + (z_2 - z_1)^2 \right]^{m/2} - (z_2 - z_1)^m \right\} dz_2 dz_1. \quad (\text{A3})$$

Where L is the largest scale (the size of the computational box, or the physical size of a cloud). It is possible to evaluate this integral changing variables from z_1 and z_2 , to $z_+ = (z_1 + z_2)/2$ and $z_- = z_2 - z_1$. With this new variables, equation A3 becomes

$$\begin{aligned} \langle [V_z(\mathbf{X}_1) - V_z(\mathbf{X}_2)]^2 \rangle &= 2 C_1 \int_0^L \int_{z_-/2}^{L-(z_-/2)} \left[(R^2 + z_-^2)^{m/2} - z_-^m \right] dz_+ dz_- \\ &= 2 C_1 \int_0^L \left[(R^2 + z_-^2)^{m/2} - z_-^m \right] (L - z_-) dz_-. \end{aligned} \quad (\text{A4})$$

The remaining integral can be solved analytically in terms of hypergeometric functions, and converge only for $m > -1$ (which is automatically satisfied since the spectrum is steep therefore with $m > 0$), yielding (a similar formula can be found in Stutzki et al. 1998):

$$\begin{aligned} \langle [V_z(\mathbf{X}_1) - V_z(\mathbf{X}_2)]^2 \rangle &= 2 C_1 L^2 \left\{ R^m {}_2F_1 \left(\frac{1}{2}, -\frac{m}{2}, \frac{3}{2}; -\frac{L^2}{R^2} \right) + \left(\frac{R^2}{L^2} \right) \frac{\left[R^m - (L^2 + R^2)^{m/2} \right]}{m+2} \right. \\ &\quad \left. - \frac{L^m (m+1) + (L^2 + R^2)^{m/2}}{m+2} \right\}. \end{aligned} \quad (\text{A5})$$

Where ${}_2F_1$ is the hypergeometric function, and has series expansion (hypergeometric series) of the form:

$${}_2F_1(a, b, c; x) = y(x) = 1 + \frac{ab}{c} \frac{x}{1!} + \frac{a(a+1)b(b+1)}{c(c+1)} \frac{x^2}{2!} + \dots \quad (A6)$$

$$c \neq 0, -1, -2, -3, \dots$$

However, for all practical purposes, we can calculate it numerically, directly from the definition in equation (A4), yet the zero point (determined by C_1) has to be estimated. At small separations ($R \ll L$), the projected structure functions is well approximated by a power-law of the form

$$\langle [V_z(\mathbf{X}_1) - V_z(\mathbf{X}_2)]^2 \rangle \approx C' R^{m+1} \quad R \ll L. \quad (A7)$$

From the structure functions of the 2D maps of integrated velocity, and column density we can compute C' , at $R = 1$, and we can estimate C from them by matching the zero point of the projected structure functions and numerical evaluation of the evaluation of equation (A3). At larger scales ($R \gg L$) equation (A5), will follow a power law of the form

$$\langle [V_z(\mathbf{X}_1) - V_z(\mathbf{X}_2)]^2 \rangle \approx C'' R^m \quad R \gg L. \quad (A8)$$

If we have enough inertial range bellow L . The spectral index m can be obtained from the 2D structure function, and verified with the 2D power spectrum. An example of a numerically integrated structure function using equation (A4) and the asymptotic in equations (A7) and (A8) is shown in Figure (7) for a structure function index of $m = 2/3$. This first panel is almost equivalent to Figure (3), where we calculate the structure function of integrated data cubes (Gaussian), but in Figure (7a) only theoretical expressions have been used, agreement of the two results provides us with a healthy verification.

A.2. Projection of a field with a shallow power spectrum

Consider a shallow density field (also isotropic), with a 3D structure function of the form (combining eqs. [4] and [12])

$$\langle (\rho(\mathbf{x}_1) - \rho(\mathbf{x}_2))^2 \rangle = 2 \left[B(0) - C_2 \left(\frac{r}{r_c} \right)^{\alpha/2} K_{\alpha/2} \left(\frac{r}{r_c} \right) \right]. \quad (A9)$$

The structure function of integrated density (column density) for this case can be written as

$$\langle [I(\mathbf{X}_1) - I(\mathbf{X}_2)]^2 \rangle = 2C_2 L \int_0^L \left[- \left(\frac{\sqrt{R^2 + z^2}}{r_c} \right)^{\alpha/2} K_{\alpha/2} \left(\frac{\sqrt{R^2 + z^2}}{r_c} \right) + \left(\frac{z}{r_c} \right)^{\alpha/2} K_{\alpha/2} \left(\frac{z}{r_c} \right) \right] dz, \quad (A10)$$

where for a shallow spectrum $\alpha < 0$. This integral is more difficult to evaluate analytically than the long-wave dominated case, but for practicality we can solve it numerically. We also find that for small scales, the result can be well approximated by a simple power-law:

$$\langle [I(\mathbf{X}_1) - I(\mathbf{X}_2)]^2 \rangle \approx C'_2 R^{m+1} \quad R \ll L, \quad (A11)$$

the zero point can be found by matching the numerical result of eq. (A11) to the calculated structure function from the data. For large separations ($R \gg L$) the resulting structure function of the integrated field will follow the asymptotic scaling of the 3D structure function:

$$\langle [I(\mathbf{X}_1) - I(\mathbf{X}_2)]^2 \rangle \approx \text{constant} = C_2'' R^{\alpha} \quad R \gg L. \quad (\text{A12})$$

In Figure 7 we also show an example of the numerical calculation of an integrated structure function using (A10) and the asymptotics in equations (A11) and (A8), for a index $\alpha = -0.5$ (corresponding to a 3D power spectrum with an index $\gamma_{3D} = -2.5$).

B. Second order structure function of unnormalized velocity centroids

Consider the structure function of the unnormalized velocity centroids (equation 26):

$$\langle [S(\mathbf{X}_1) - S(\mathbf{X}_2)]^2 \rangle = \left\langle \left(\alpha \int v_z(\mathbf{x}_1) \rho(\mathbf{x}_1) dz - \alpha \int v_z(\mathbf{x}_2) \rho(\mathbf{x}_2) dz \right)^2 \right\rangle. \quad (\text{B1})$$

As described in §2.4 (and in Lazarian 1995), we can rewrite last line as in equations (27) and (28), that we rewrite here:

$$\langle [S(\mathbf{X}_1) - S(\mathbf{X}_2)]^2 \rangle = \alpha^2 \iint dz_1 dz_2 [D(\mathbf{r}) - D(\mathbf{r})|_{\mathbf{X}_1=\mathbf{X}_2}], \quad (\text{B2})$$

where

$$D(\mathbf{r}) = \langle (v_z(\mathbf{x}_1)\rho(\mathbf{x}_1) - v_z(\mathbf{x}_2)\rho(\mathbf{x}_2))^2 \rangle. \quad (\text{B3})$$

Using the definitions² $v_z = v_0 + \tilde{v}_z$, $\rho = \rho_0 + \tilde{\rho}$ in (B3) we have

$$\begin{aligned} D(\mathbf{r}) &= \langle [v_0\rho_0 + \tilde{v}_z(\mathbf{x}_1)\rho_0 + v_0\tilde{\rho}(\mathbf{x}_1) + \tilde{v}_z(\mathbf{x}_1)\tilde{\rho}(\mathbf{x}_1) - v_0\rho_0 + \tilde{v}_z(\mathbf{x}_2)\rho_0 + v_0\tilde{\rho}(\mathbf{x}_2) + \tilde{v}_z(\mathbf{x}_2)\tilde{\rho}(\mathbf{x}_2)]^2 \rangle \\ &= \langle \{v_0 [\tilde{\rho}(\mathbf{x}_1) - \tilde{\rho}(\mathbf{x}_2)] + \rho_0 [\tilde{v}_z(\mathbf{x}_1) - \tilde{v}_z(\mathbf{x}_2)] + [\tilde{v}_z(\mathbf{x}_1)\tilde{\rho}(\mathbf{x}_1) - \tilde{v}_z(\mathbf{x}_1)\tilde{\rho}(\mathbf{x}_2)] \}^2 \rangle. \end{aligned} \quad (\text{B4})$$

Expanding this last expression yields:

$$\begin{aligned} D(\mathbf{r}) &= \langle v_0^2 [\rho(\mathbf{x}_1) - \rho(\mathbf{x}_2)]^2 + \rho_0^2 [v_z(\mathbf{x}_1) - v_z(\mathbf{x}_2)]^2 + [\tilde{v}_z(\mathbf{x}_1)\tilde{\rho}(\mathbf{x}_1) - \tilde{v}_z(\mathbf{x}_2)\tilde{\rho}(\mathbf{x}_2)] \\ &\quad + 2v_0\rho_0 [\rho(\mathbf{x}_1) - \rho(\mathbf{x}_2)] [v_z(\mathbf{x}_1) - v_z(\mathbf{x}_2)] + 2\rho_0 [v_z(\mathbf{x}_1) - v_z(\mathbf{x}_2)] [\tilde{v}_z(\mathbf{x}_1)\tilde{\rho}(\mathbf{x}_1) - \tilde{v}_z(\mathbf{x}_2)\tilde{\rho}(\mathbf{x}_2)] \\ &\quad + 2v_0 [v_z(\mathbf{x}_1) - v_z(\mathbf{x}_2)] [\tilde{v}_z(\mathbf{x}_1)\tilde{\rho}(\mathbf{x}_1) - \tilde{v}_z(\mathbf{x}_2)\tilde{\rho}(\mathbf{x}_2)] \rangle \\ &= v_0^2 \langle [\rho(\mathbf{x}_1) - \rho(\mathbf{x}_2)]^2 \rangle + \rho_0^2 \langle [v_z(\mathbf{x}_1) - v_z(\mathbf{x}_2)]^2 \rangle + \langle [\tilde{v}_z(\mathbf{x}_1)\tilde{\rho}(\mathbf{x}_1) - \tilde{v}_z(\mathbf{x}_2)\tilde{\rho}(\mathbf{x}_2)]^2 \rangle + \\ &\quad 2v_0\rho_0 \langle [\rho(\mathbf{x}_1) - \rho(\mathbf{x}_2)] [v_z(\mathbf{x}_1) - v_z(\mathbf{x}_2)] \rangle + 2\rho_0 \langle [v_z(\mathbf{x}_1) - v_z(\mathbf{x}_2)] [\tilde{v}_z(\mathbf{x}_1)\tilde{\rho}(\mathbf{x}_1) - \tilde{v}_z(\mathbf{x}_2)\tilde{\rho}(\mathbf{x}_2)] \rangle \\ &\quad + 2v_0 \langle [\rho(\mathbf{x}_1) - \rho(\mathbf{x}_2)] [\tilde{v}_z(\mathbf{x}_1)\tilde{\rho}(\mathbf{x}_1) - \tilde{v}_z(\mathbf{x}_2)\tilde{\rho}(\mathbf{x}_2)] \rangle. \end{aligned} \quad (\text{B5})$$

²Notice that for a homogeneous and thermalized media the thermal velocity does not contribute to the velocity fluctuations. This is because the thermal profile is symmetric and its first moment vanishes. Therefore integration of the line profile will reveal the asymmetries due to turbulence.

Now consider the cross terms one by one: the third term in equation (B5) is

$$\left\langle [\tilde{v}_z(\mathbf{x}_1)\tilde{\rho}(\mathbf{x}_1) - \tilde{v}_z(\mathbf{x}_2)\tilde{\rho}(\mathbf{x}_2)]^2 \right\rangle = \left\langle \tilde{v}_z^2(\mathbf{x}_1)\tilde{\rho}^2(\mathbf{x}_1) \right\rangle + \left\langle \tilde{v}_z^2(\mathbf{x}_2)\tilde{\rho}^2(\mathbf{x}_2) \right\rangle - 2 \left\langle \tilde{v}_z(\mathbf{x}_1)\tilde{\rho}(\mathbf{x}_1)\tilde{v}_z(\mathbf{x}_2)\tilde{\rho}(\mathbf{x}_2) \right\rangle. \quad (\text{B6})$$

Relating the fourth order moments with the second order, using the Millionshikov hypothesis³ (see Monin & Yaglom 1975), $\langle h_1 h_2 h_3 h_4 \rangle \approx \langle h_1 h_2 \rangle \langle h_3 h_4 \rangle + \langle h_1 h_3 \rangle \langle h_2 h_4 \rangle + \langle h_1 h_4 \rangle \langle h_2 h_3 \rangle$ we have:

$$\left\langle \tilde{v}_z^2(\mathbf{x}_1)\tilde{\rho}^2(\mathbf{x}_1) \right\rangle = \left\langle \tilde{v}_z(\mathbf{x}_1)\tilde{\rho}(\mathbf{x}_1)\tilde{v}_z(\mathbf{x}_1)\tilde{\rho}(\mathbf{x}_1) \right\rangle \approx \left\langle \tilde{v}_z^2(\mathbf{x}_1) \right\rangle \left\langle \tilde{\rho}^2(\mathbf{x}_1) \right\rangle + 2 \left\langle \tilde{v}_z(\mathbf{x}_1)\tilde{\rho}(\mathbf{x}_1) \right\rangle^2, \quad (\text{B7a})$$

$$\left\langle \tilde{v}_z^2(\mathbf{x}_2)\tilde{\rho}^2(\mathbf{x}_2) \right\rangle = \left\langle \tilde{v}_z(\mathbf{x}_2)\tilde{\rho}(\mathbf{x}_2)\tilde{v}_z(\mathbf{x}_2)\tilde{\rho}(\mathbf{x}_2) \right\rangle \approx \left\langle \tilde{v}_z^2(\mathbf{x}_2) \right\rangle \left\langle \tilde{\rho}^2(\mathbf{x}_2) \right\rangle + 2 \left\langle \tilde{v}_z(\mathbf{x}_2)\tilde{\rho}(\mathbf{x}_2) \right\rangle^2, \quad (\text{B7b})$$

$$\begin{aligned} 2 \left\langle \tilde{v}_z(\mathbf{x}_1)\tilde{\rho}(\mathbf{x}_1)\tilde{v}_z(\mathbf{x}_2)\tilde{\rho}(\mathbf{x}_2) \right\rangle &\approx 2 \left\langle \tilde{v}_z(\mathbf{x}_1)\tilde{\rho}(\mathbf{x}_1) \right\rangle \left\langle \tilde{v}_z(\mathbf{x}_2)\tilde{\rho}(\mathbf{x}_2) \right\rangle \\ &\quad + 2 \left\langle \tilde{v}_z(\mathbf{x}_1)\tilde{v}_z(\mathbf{x}_2) \right\rangle \left\langle \tilde{\rho}(\mathbf{x}_1)\tilde{\rho}(\mathbf{x}_2) \right\rangle \\ &\quad + 2 \left\langle \tilde{v}_z(\mathbf{x}_1)\tilde{\rho}(\mathbf{x}_2) \right\rangle \left\langle \tilde{v}_z(\mathbf{x}_2)\tilde{\rho}(\mathbf{x}_1) \right\rangle. \end{aligned} \quad (\text{B7c})$$

Combining the last three lines, using

$$\begin{aligned} \left\langle [v_z(\mathbf{x}_1) - v_z(\mathbf{x}_2)]^2 \right\rangle &= \left\langle \tilde{v}_z^2(\mathbf{x}_1) \right\rangle - 2 \left\langle \tilde{v}_z(\mathbf{x}_1)\tilde{v}_z(\mathbf{x}_2) \right\rangle + \left\langle \tilde{v}_z^2(\mathbf{x}_2) \right\rangle \\ &= 2 \left\langle \tilde{v}_z^2 \right\rangle - 2 \left\langle \tilde{v}_z(\mathbf{x}_1)\tilde{v}_z(\mathbf{x}_2) \right\rangle \end{aligned} \quad (\text{B8a})$$

$$\Rightarrow \left\langle \tilde{v}_z(\mathbf{x}_1)\tilde{v}_z(\mathbf{x}_2) \right\rangle = \left\langle \tilde{v}_z^2 \right\rangle - \frac{1}{2} \left\langle [v_z(\mathbf{x}_1) - v_z(\mathbf{x}_2)]^2 \right\rangle \quad (\text{B8b})$$

$$\Rightarrow \left\langle \tilde{\rho}(\mathbf{x}_1)\tilde{\rho}(\mathbf{x}_2) \right\rangle = \left\langle \tilde{\rho}^2 \right\rangle - \frac{1}{2} \left\langle [\rho(\mathbf{x}_1) - \rho(\mathbf{x}_2)]^2 \right\rangle, \quad (\text{B8c})$$

together with $\langle \tilde{v}_z(\mathbf{x}_1)\tilde{\rho}(\mathbf{x}_1) \rangle = \langle \tilde{v}_z(\mathbf{x}_2)\tilde{\rho}(\mathbf{x}_2) \rangle = 0$, $\langle \tilde{v}_z^2(\mathbf{x}_1) \rangle = \langle \tilde{v}_z^2(\mathbf{x}_2) \rangle = \langle \tilde{v}_z^2 \rangle$, and $\langle \tilde{\rho}^2(\mathbf{x}_1) \rangle = \langle \tilde{\rho}^2(\mathbf{x}_2) \rangle = \langle \tilde{\rho}^2 \rangle$ equation (B6) reduces to:

$$\begin{aligned} \left\langle [\tilde{v}_z(\mathbf{x}_1)\tilde{\rho}(\mathbf{x}_1) - \tilde{v}_z(\mathbf{x}_2)\tilde{\rho}(\mathbf{x}_2)]^2 \right\rangle &\approx 2 \left\langle \tilde{v}_z^2 \right\rangle \left\langle \tilde{\rho}^2 \right\rangle - 2 \left\langle \tilde{v}_z(\mathbf{x}_1)\tilde{\rho}(\mathbf{x}_2) \right\rangle \left\langle \tilde{v}_z(\mathbf{x}_2)\tilde{\rho}(\mathbf{x}_1) \right\rangle \\ &\quad - 2 \left\{ \left[\left\langle \tilde{v}_z^2 \right\rangle - \frac{1}{2} \left\langle [v_z(\mathbf{x}_1) - v_z(\mathbf{x}_2)]^2 \right\rangle \right] \right. \\ &\quad \left. \left[\left\langle \tilde{\rho}^2 \right\rangle - \frac{1}{2} \left\langle [\rho(\mathbf{x}_1) - \rho(\mathbf{x}_2)]^2 \right\rangle \right] \right\}. \end{aligned} \quad (\text{B9})$$

To treat terms of the form $\langle \tilde{\rho}\tilde{v}_z \rangle$ we can generalize the correlation function defined in equation (1), considering a four-dimensional vector of the form $[v_x(\mathbf{x}), v_y(\mathbf{x}), v_z(\mathbf{x}), \rho(\mathbf{x})]$. Thus the resulting cross correlation between the z component of the velocity and the density is

$$B_{z\rho}(\mathbf{r}) = \langle v_z(\mathbf{x}_1)\rho(\mathbf{x}_2) \rangle. \quad (\text{B10})$$

Similarly to the derivation of equation (6a) it can be shown that for an isotropic (four-dimensional, $[v_x(\mathbf{x}), v_y(\mathbf{x}), v_z(\mathbf{x}), \rho(\mathbf{x})]$) field $B_{j\rho}(r) = B_{L\rho}(r)r_j/r$, and $B_{\rho j}(r) = B_{\rho L}(r)r_j/r = -B_{L\rho}(r)r_j/r$.

³Evidently, this hypothesis is identically true for Gaussian fields, strongly non Gaussian fields may show deviations.

Therefore $\langle \tilde{v}_z(\mathbf{x}_1)\tilde{\rho}(\mathbf{x}_2) \rangle = -\langle \tilde{v}_z(\mathbf{x}_2)\tilde{\rho}(\mathbf{x}_1) \rangle$, and equation (B9) simplifies to

$$\begin{aligned} \left\langle [\tilde{v}_z(\mathbf{x}_1)\tilde{\rho}(\mathbf{x}_1) - \tilde{v}_z(\mathbf{x}_2)\tilde{\rho}(\mathbf{x}_2)]^2 \right\rangle &\approx 2\langle \tilde{v}_z(\mathbf{x}_1)\tilde{\rho}(\mathbf{x}_2) \rangle^2 + \langle \tilde{v}_z^2 \rangle \left\langle [\rho(\mathbf{x}_1) - \rho(\mathbf{x}_2)]^2 \right\rangle \\ &\quad + \langle \tilde{\rho}^2 \rangle \left\langle [v_z(\mathbf{x}_1) - v_z(\mathbf{x}_2)]^2 \right\rangle \\ &\quad - \frac{1}{2} \left\langle [v_z(\mathbf{x}_1) - v_z(\mathbf{x}_2)]^2 \right\rangle \left\langle [\rho(\mathbf{x}_1) - \rho(\mathbf{x}_2)]^2 \right\rangle. \end{aligned} \quad (\text{B11})$$

The next term of equation (B5)

$$2v_0\rho_0 \langle [\rho(\mathbf{x}_1) - \rho(\mathbf{x}_2)] [v_z(\mathbf{x}_1) - v_z(\mathbf{x}_2)] \rangle = 0, \quad (\text{B12})$$

as shown in Monin & Yaglom (1975).

The fifth term in equation (B5) is:

$$\begin{aligned} 2\rho_0 \langle [\tilde{v}_z(\mathbf{x}_1) - \tilde{v}_z(\mathbf{x}_2)] [\tilde{v}_z(\mathbf{x}_1)\tilde{\rho}(\mathbf{x}_1) - \tilde{v}_z(\mathbf{x}_2)\tilde{\rho}(\mathbf{x}_2)] \rangle &= 2\rho_0 \langle \tilde{v}_z(\mathbf{x}_1)\tilde{\rho}(\mathbf{x}_1) \rangle + 2\rho_0 \langle \tilde{v}_z(\mathbf{x}_2)\tilde{\rho}(\mathbf{x}_2) \rangle \\ &\quad - 2\rho_0 \langle \tilde{v}_z(\mathbf{x}_1)\tilde{v}_z(\mathbf{x}_2)\tilde{\rho}(\mathbf{x}_1) \rangle \\ &\quad - 2\rho_0 \langle \tilde{v}_z(\mathbf{x}_1)\tilde{v}_z(\mathbf{x}_2)\tilde{\rho}(\mathbf{x}_2) \rangle \end{aligned} \quad (\text{B13})$$

For the terms with correlations of third order we need to introduce the so called two-point third order moments

$$B_{ij,l}(\mathbf{r}) = \langle u_i(\mathbf{x}_1)u_j(\mathbf{x}_1)u_l(\mathbf{x}_2) \rangle. \quad (\text{B14})$$

Which can be generalized to include cross correlations of density and velocity as explained for equation (B10). Analogously to the second order cross correlations, considering an isotropic (four dimensional) field, and decomposing it in terms of longitudinal and lateral components. It can be shown (for more details we refer the reader to Monin & Yaglom 1975) that

$$\langle \tilde{v}_z(\mathbf{x}_1)\tilde{v}_z(\mathbf{x}_2)\tilde{\rho}(\mathbf{x}_1) \rangle = \langle \tilde{v}_z(\mathbf{x}_1)\tilde{v}_z(\mathbf{x}_2)\tilde{\rho}(\mathbf{x}_2) \rangle, \quad (\text{B15a})$$

$$\langle \tilde{v}_z(\mathbf{x}_1)\tilde{\rho}_z(\mathbf{x}_1)\tilde{\rho}(\mathbf{x}_2) \rangle = -\langle \tilde{v}_z(\mathbf{x}_1)\tilde{\rho}_z(\mathbf{x}_1)\tilde{\rho}(\mathbf{x}_2) \rangle. \quad (\text{B15b})$$

Equation (B15a), combined with $\langle \tilde{\rho}(\mathbf{x}_1)\tilde{v}_z^2(\mathbf{x}_1) \rangle = \langle \tilde{\rho}(\mathbf{x}_2)\tilde{v}_z^2(\mathbf{x}_2) \rangle$ reduces equation (B13) to:

$$\begin{aligned} 2\rho_0 \langle [\tilde{v}_z(\mathbf{x}_1) - \tilde{v}_z(\mathbf{x}_2)] [\tilde{v}_z(\mathbf{x}_1)\tilde{\rho}(\mathbf{x}_1) - \tilde{v}_z(\mathbf{x}_2)\tilde{\rho}(\mathbf{x}_2)] \rangle &= 4\rho_0 \langle \tilde{\rho}(\mathbf{x}_1)\tilde{v}_z^2(\mathbf{x}_1) \rangle \\ &\quad - 4\rho_0 \langle \tilde{v}_z(\mathbf{x}_1)\tilde{v}_z(\mathbf{x}_2)\tilde{\rho}(\mathbf{x}_1) \rangle. \end{aligned} \quad (\text{B16})$$

Similarly the last term in equation (B5) can be written

$$\begin{aligned} 2v_0 \langle [\rho(\mathbf{x}_1) - \rho(\mathbf{x}_2)] [\tilde{v}_z(\mathbf{x}_1)\tilde{\rho}(\mathbf{x}_1) - \tilde{v}_z(\mathbf{x}_2)\tilde{\rho}(\mathbf{x}_2)] \rangle &= 2v_0 \langle \tilde{v}_z(\mathbf{x}_1)\tilde{\rho}^2(\mathbf{x}_1) \rangle \\ &\quad + 2v_0 \langle \tilde{v}_z(\mathbf{x}_2)\tilde{\rho}^2(\mathbf{x}_2) \rangle \\ &\quad - 2v_0 \langle \tilde{\rho}(\mathbf{x}_1)\tilde{\rho}(\mathbf{x}_2)\tilde{v}_z(\mathbf{x}_1) \rangle \\ &\quad - 2v_0 \langle \tilde{\rho}(\mathbf{x}_1)\tilde{\rho}(\mathbf{x}_2)\tilde{v}_z(\mathbf{x}_2) \rangle. \end{aligned} \quad (\text{B17})$$

But in this case, $\langle \tilde{v}_z(\mathbf{x}_1)\tilde{\rho}^2(\mathbf{x}_1) \rangle = \langle \tilde{v}_z(\mathbf{x}_2)\tilde{\rho}^2(\mathbf{x}_2) \rangle = 0$, combined with equation (B15b), yields

$$2v_0 \langle [\rho(\mathbf{x}_1) - \rho(\mathbf{x}_2)] [\tilde{v}_z(\mathbf{x}_1)\tilde{\rho}(\mathbf{x}_1) - \tilde{v}_z(\mathbf{x}_2)\tilde{\rho}(\mathbf{x}_2)] \rangle = 0. \quad (\text{B18})$$

Finally, combining (B5, B11, B12, B16, B18)

$$\begin{aligned} D \approx & v_0^2 \langle [\rho(\mathbf{x}_1) - \rho(\mathbf{x}_2)]^2 \rangle + \rho_0^2 \langle [v_z(\mathbf{x}_1) - v_z(\mathbf{x}_2)]^2 \rangle + 2 \langle \tilde{v}_z(\mathbf{x}_1)\tilde{\rho}(\mathbf{x}_2) \rangle^2 \\ & + \langle \tilde{v}_z^2 \rangle \langle [\rho(\mathbf{x}_1) - \rho(\mathbf{x}_2)]^2 \rangle + \langle \tilde{\rho}^2 \rangle \langle [v_z(\mathbf{x}_1) - v_z(\mathbf{x}_2)]^2 \rangle \\ & - \frac{1}{2} \langle [v_z(\mathbf{x}_1) - v_z(\mathbf{x}_2)]^2 \rangle \langle [\rho(\mathbf{x}_1) - \rho(\mathbf{x}_2)]^2 \rangle + 4\rho_0 \langle \tilde{\rho}(\mathbf{x}_1)\tilde{v}_z^2(\mathbf{x}_1) \rangle \\ & - 4\rho_0 \langle \tilde{v}_z(\mathbf{x}_1)\tilde{v}_z(\mathbf{x}_2)\tilde{\rho}(\mathbf{x}_1) \rangle. \end{aligned} \quad (\text{B19})$$

Grouping some terms:

$$\begin{aligned} D \approx & \langle \tilde{\rho}^2 + \rho_0^2 \rangle \langle [v_z(\mathbf{x}_1) - v_z(\mathbf{x}_2)]^2 \rangle + \langle \tilde{v}^2 + v_0^2 \rangle \langle [\rho(\mathbf{x}_1) - \rho(\mathbf{x}_2)]^2 \rangle \\ & - \frac{1}{2} \langle [v_z(\mathbf{x}_1) - v_z(\mathbf{x}_2)]^2 \rangle \langle [\rho(\mathbf{x}_1) - \rho(\mathbf{x}_2)]^2 \rangle + 2 \langle \tilde{v}_z(\mathbf{x}_1)\tilde{\rho}(\mathbf{x}_2) \rangle^2 \\ & + 4\rho_0 \langle \tilde{\rho}(\mathbf{x}_1)\tilde{v}_z^2(\mathbf{x}_1) \rangle - 4\rho_0 \langle \tilde{v}_z(\mathbf{x}_1)\tilde{v}_z(\mathbf{x}_2)\tilde{\rho}(\mathbf{x}_1) \rangle. \end{aligned} \quad (\text{B20})$$

Lastly, with $\langle \rho^2 \rangle = \langle \tilde{\rho} + \rho_0^2 \rangle$, and $\langle v^2 \rangle = \langle \tilde{v}^2 + v_0^2 \rangle$ we arrive to equations (29) and (31):

$$\begin{aligned} D \approx & \langle \rho^2 \rangle \langle [v_z(\mathbf{x}_1) - v_z(\mathbf{x}_2)]^2 \rangle + \langle v^2 \rangle \langle [\rho(\mathbf{x}_1) - \rho(\mathbf{x}_2)]^2 \rangle \\ & - \frac{1}{2} \langle [v_z(\mathbf{x}_1) - v_z(\mathbf{x}_2)]^2 \rangle \langle [\rho(\mathbf{x}_1) - \rho(\mathbf{x}_2)]^2 \rangle + c(\mathbf{r}), \end{aligned} \quad (\text{B21})$$

with

$$c(\mathbf{r}) = 2 \langle \tilde{v}_z(\mathbf{x}_1)\tilde{\rho}(\mathbf{x}_2) \rangle^2 + 4\rho_0 \langle \tilde{\rho}(\mathbf{x}_1)\tilde{v}_z^2(\mathbf{x}_1) \rangle - 4\rho_0 \langle \tilde{v}_z(\mathbf{x}_1)\tilde{v}_z(\mathbf{x}_2)\tilde{\rho}(\mathbf{x}_1) \rangle. \quad (\text{B22})$$

C. Power spectra of a field integrated along the line of sight

Consider the structure function of the velocity field, projected along the direction related to the LOS. We can exemplify this case for $I2(\mathbf{R}) \gg I3(\mathbf{R})$, approximating the structure function of MVCs as

$$M(\mathbf{R}) \approx \alpha^2 \langle \rho^2 \rangle \int \int dz_1 dz_2 \left(\langle [v_z(\mathbf{x}_1) - v_z(\mathbf{x}_2)]^2 \rangle - \left. \langle [v_z(\mathbf{x}_1) - v_z(\mathbf{x}_2)]^2 \rangle \right|_{\mathbf{x}_1=\mathbf{x}_2} \right), \quad (\text{C1})$$

which is precisely the integration of the velocity structure function analogous to what we show for the density structure function in equation (20).

Using

$$\langle [v_z(\mathbf{x}_1) - v_z(\mathbf{x}_2)]^2 \rangle = 2B_{zz}(0) - 2B_{zz}(\mathbf{r}), \quad (\text{C2a})$$

$$\langle [v_z(\mathbf{x}_1) - v_z(\mathbf{x}_2)] \rangle|_{\mathbf{x}_1=\mathbf{x}_2} = 2B_{zz}(0) - 2B_{zz}(\mathbf{r})|_{\mathbf{x}_1=\mathbf{x}_2}. \quad (\text{C2b})$$

And, combining the last two equations with equation (5) of the paper:

$$\begin{aligned} M(\mathbf{R}) &= 2\alpha^2 \langle \rho^2 \rangle \iint dz_1 dz_2 [-B_{zz}(\mathbf{r}) + 2B_{zz}(\mathbf{r})|_{\mathbf{X}_1=\mathbf{X}_2}] \\ &= 2\alpha^2 \langle \rho^2 \rangle \iint dz_1 dz_2 \left[- \int d^3\mathbf{k} e^{i\mathbf{k}\cdot\mathbf{r}} F_{zz}(\mathbf{k}) + \int d^3\mathbf{k} e^{ik_z(z_2-z_1)} F_{zz}(\mathbf{k}) \right]. \end{aligned} \quad (\text{C3})$$

Taking the 2D Fourier transform of the last expression

$$\begin{aligned} P_{2D}(\mathbf{K}) &= \frac{1}{4\pi^2} \int d^2\mathbf{R} e^{-i\mathbf{K}\cdot\mathbf{R}} M(\mathbf{R}) \\ P_{2D}(\mathbf{K}) &= \frac{2\alpha^2 \langle \rho^2 \rangle}{4\pi^2} \int d^2\mathbf{R} e^{-i\mathbf{K}\cdot\mathbf{R}} \iint dz_1 dz_2 \left[- \int d^3\mathbf{k} e^{i\mathbf{k}\cdot\mathbf{r}} F_{zz}(\mathbf{k}) + \int d^3\mathbf{k} e^{ik_z(z_2-z_1)} F_{zz}(\mathbf{k}) \right], \end{aligned} \quad (\text{C4})$$

using $\mathbf{k} = (\mathbf{K}, k_z)$, and $\mathbf{r} = (\mathbf{R}, z_2 - z_1)$:

$$\begin{aligned} P_{2D}(\mathbf{K}) &= \frac{\alpha^2 \langle \rho^2 \rangle}{2\pi^2} \int d^2\mathbf{R} e^{-i\mathbf{K}\cdot\mathbf{R}} \iint dz_1 dz_2 \\ &\quad \left[- \int d^3\mathbf{k} e^{i\mathbf{K}\cdot\mathbf{R} + ik_z(z_2-z_1)} F_{zz}(\mathbf{K}, k_z) + \int d^3\mathbf{k} e^{ik_z(z_2-z_1)} F_{zz}(\mathbf{K}, k_z) \right], \end{aligned} \quad (\text{C5})$$

interchanging the order of integration:

$$\begin{aligned} P_{2D}(\mathbf{K}) &= \frac{\alpha^2 \langle \rho^2 \rangle}{2\pi^2} \iint dz_1 dz_2 \int d^3\mathbf{k}' \\ &\quad \left[- \int d^2\mathbf{R} e^{i(\mathbf{K}' - \mathbf{K})\cdot\mathbf{R} + ik'_z(z_2-z_1)} F_{zz}(\mathbf{K}', k'_z) + \int d^2\mathbf{R} e^{-\mathbf{K}\cdot\mathbf{R} + ik'_z(z_2-z_1)} F_{zz}(\mathbf{K}', k'_z) \right] \end{aligned} \quad (\text{C6})$$

After performing the integral over \mathbf{R} :

$$P_{2D}(\mathbf{K}) = 2\alpha^2 \langle \rho^2 \rangle \iint dz_1 dz_2 \int d^3\mathbf{k}' \left[-e^{ik'_z(z_2-z_1)} \delta(\mathbf{K}' - \mathbf{K}) F_{zz}(\mathbf{K}', k'_z) + e^{ik'_z(z_2-z_1)} \delta(\mathbf{K}) F_{zz}(\mathbf{K}', k'_z) \right]. \quad (\text{C7})$$

Now performing the integral over \mathbf{K}' :

$$P_{2D}(\mathbf{K}) = 2\alpha^2 \langle \rho^2 \rangle \iint dz_1 dz_2 \left[- \int dk_z e^{ik'_z(z_2-z_1)} F_{zz}(-\mathbf{K}, k'_z) + \delta(\mathbf{K}) \int d^3\mathbf{k}' e^{ik'_z(z_2-z_1)} F_{zz}(\mathbf{K}', k'_z) \right]. \quad (\text{C8})$$

Changing variables $z_+ = (z_1 + z_2)/2$, $z_- = z_2 - z_1$, using $F_{zz}(-\mathbf{k}) = F_{zz}(\mathbf{k})$, and performing the integral over z_- :

$$P_{2D}(\mathbf{K}) = 8\pi\alpha^2 \langle \rho^2 \rangle \iint dz_+ \left[\int dk_z \delta(k_z) F_{zz}(\mathbf{K}, k'_z) + \delta(\mathbf{K}) \int d^3\mathbf{k}' \delta(k_z) F_{zz}(\mathbf{K}', k'_z) \right], \quad (\text{C9})$$

now we do the integral over k'_z , then finally over z_+ :

$$\begin{aligned} P_{2D}(\mathbf{K}) &= 8\pi\alpha^2 \langle \rho^2 \rangle \int dz_+ \left[-F_{zz}(\mathbf{K}, 0) + \delta(\mathbf{K}) \int d^3\mathbf{K}' F_{zz}(\mathbf{K}', 0) \right] \\ &= 4\pi\alpha^2 \langle \rho^2 \rangle L F_{zz}(\mathbf{K}, 0) + \text{const } \delta(\mathbf{K}), \end{aligned} \quad (\text{C10})$$

lastly, replacing $k_z = 0$, in equation (6c) $F_{zz}(\mathbf{K}, 0) = F_{NN}(K)$, we recover from the integrated structure function the spectrum of the solenoidal component of the velocity:

$$P_{2D}(\mathbf{K}) = 4\pi\alpha^2 \langle \rho^2 \rangle L F_{NN}(K) + \text{const } \delta(\mathbf{K}). \quad (\text{C11})$$

REFERENCES

Armstrong, J. M., Rickett, B. J., & Spangler, S. R. 1995, *ApJ*, 443, 209

Bensch, F., Stutzki, J., & Ossenkopf, V. 2001, *A&A*, 366, 636

Brunt, C. M., Heyer, M. H., Vázquez-Semadeni, E., & Pichardo, B. 2003, *ApJ*, 595, 824

Brunt, C. M., & Heyer, M. H. 2002(a), *ApJ*, 556, 276

Brunt, C. M., & Heyer, M. H. 2002(b), *ApJ*, 556, 289

Brunt, C. M., & Mac Low, M. 2004, *ApJ*, 604, 196

Cho, J., & Lazarian, A. 2002, *Phys. Rev. Lett.*, 88, 5001

Cho, J., & Lazarian, A. 2003a, in *Acoustic emission and scattering by turbulent flows*, ed. M. Rast (Berlin: Springer), in press, astro-ph/0301462

Cho, J., & Lazarian, A. 2003b, *MNRAS*, 345, 325

Cho, J., Lazarian, A., Vishniac E. T. 2003, in *Turbulence and Magnetic Fields in Astrophysics*, ed. E. Falgarone, & T. Passot (Berlin: Springer), 53

Cordes, J. 1999, in *Interstellar Turbulence*, ed. José Franco & Alberto Carramiñana, (Cambridge: Cambridge Univ. Press), p.33

Deshpande, A. A., Dwarakanath, K. S., & Goss, W. M. 2000, *ApJ*, 543, 227

Dickman, R. L., & Kleiner, S. C. 1985, *ApJ*, 295, 479

Esquivel, A., Lazarian, A., Pogosyan, D., & Cho, J. 2003, *MNRAS*, 342, 325

Jackson, J. M., Bania, T. M., Simon, R., Kolpack, M., Clemens, D. P., & Heyer, M. 2002, *ApJ*, 566, L81

Kitamura, Y., Sunada, K., Hayashi, M., & Hasegawa, T. 1993, *ApJ*, 413, 221

Kleiner, S. C., & Dickman, R. L. 1985, *ApJ*, 295, 466

Larson, R. B. 1981, *MNRAS*, 194, 809

Larson, R. B. 1992, *MNRAS*, 641

Lazarian, A. 1995, A&A, 293, 507

Lazarian, A. 1999, in Plasma Turbulence and Energetic Particles in Astrophysics, ed. M. Ostrowski, & R. Schlickeiser, (Krakow: Jagiellonian Univ) , 28

Lazarian, A., & Esquivel, A. 2003, ApJ, L37 (LE03)

Lazarian, A., & Pogosyan, D. 2000, ApJ, 537, 72

Lazarian, A., Pogosyan, D., Vázquez-Semadeni, E., & Pichardo, B. 2001, ApJ, 555, 130

Li, D., & Goldsmith, P. F. 2003, ApJ, 585, 823

Matthaeus, W. M., Ghosh, S., Oughton, S., & Roberts, D. A. 1996, J. Geophys. Res., 101, 7619

Mc Low, M. M., & Ossenkopf, V. 2000, A&A, 353, 339

Miesch, M. S., & Bally, J. 1994, ApJ, 429, 645

Minter, A. 2002, ASP Conf. Ser. 276: Seeing Through the Dust: The Detection of HI and the Exploration of the ISM in Galaxies, 221

Miville-Deschénes, M.-A., Levrier, F., & Falgarone, E. 2003, ApJ, 593, 831

Monin, A. S., & Yaglom, A. M. 1975, Statistical fluid dynamics: mechanics of turbulence, Vol. 2., (Cambridge: MIT Press)

Munch, G. 1958, Rev. Mod. Phys., 30, 1035

Narayan, R., & Goodman, J. 1989, MNRAS, 238, 963

Ossenkopf, V., & Mc Low, M. M. 2002, A&A, 390, 307

Padoan, P., Rosolowsky, E. W., & Goodman A. A. 2001, ApJ, 547, 862

Porter, D., Woodward, P., & Pouquet, A. 1998, Phys. of Fluids, 10, 237

Rosolowsky, E. W., Goodman, A. A., Wilner, D. J., & Williams, J. P. 1999, ApJ, 524, 887

Scalo, J. M. 1984, ApJ, 277, 556

Scalo, J. M. 1987, in Interstellar Processes, ed. D. F. Hollenbach & H. A. Thronson (Dordrecht: Reidel), 349

Spangler, S. R., & Gwinn, C. R. 1990, ApJ, 353, L29

Spoelstra, T. A. T. 1972, A&A, 21, 61

Stanimirović, S., & Lazarian, A., 2001, ApJ, 551, 53

Stenholm, L.G. 1990, A&A, 232, 495

Stutzki, J., Bensch, F., Heithausen, A., Ossenkopf, V., & Zielinsky, M. 1998, A&A, 336, 697

Vázquez-Semadeni, E., Ostriker, E.C., Passot, T., Gammie, C.F., & Stone, J.M. 2000, in Protostars and Planets IV, eds. V. Mannings et al. (Tucson: University of Arizona Press), p.3

Vestuto, J.G., Ostriker, E.C., & Stone, J.M. 2003, ApJ, 590, 858

von Hoerner, S. 1951, Zeitschrift für Astrophysics, 30, 17

Table 1. Parameters of the four runs used.

Run	$\langle B \rangle$	$\langle \text{gas pressure} \rangle$	rms v	Mach #	$\langle S^2 \rangle / (\langle v_z^2 \rangle \langle f^2 \rangle)$
216B1p2	1.0	2.0	0.6 – 0.7	~ 0.5	93.9
216iM2cxc	1.0	0.1	0.6 – 0.7	~ 2.5	4.6
216B01P01	0.1	0.1	~ 0.7	~ 2.5	4.2
216M7	1.0	0.01	0.6 – 0.7	~ 7	2.2

Table 2. Three-dimensional spectral indices measured from Figure 4.

Run	Density		LOS Velocity	
	γ_{3D}	m	γ_{3D}	m
216B1p2	–3.8	0.6	–4.1	0.8
216iM2cxc	–3.5	0.5	–3.9	0.6
216B01P01	–3.3	0.3	–4.1	0.9
216M7	–2.8*	0.2*	–4.4	0.8

*The measured power spectrum index in this case corresponds to a *shallow* case, therefore the structure function is not expected to follow a power-law but the correlation function. Therefore the value quoted for m has no physical relevance.

Table 3. Spectral indices measured from Figure 5.

Run	Integrated Density	Integrated Velocity	Unnormalized Centroids	Normalized Centroids	Modified Centroids
216B1p2	1.2	1.6	1.5	1.5	1.5
216iM2cxc	1.2	1.4	1.3	1.3	1.4
216B01P01	0.9	1.6	1.3	1.5	1.6
216M7	0.8	1.6	1.1	1.3	2.6

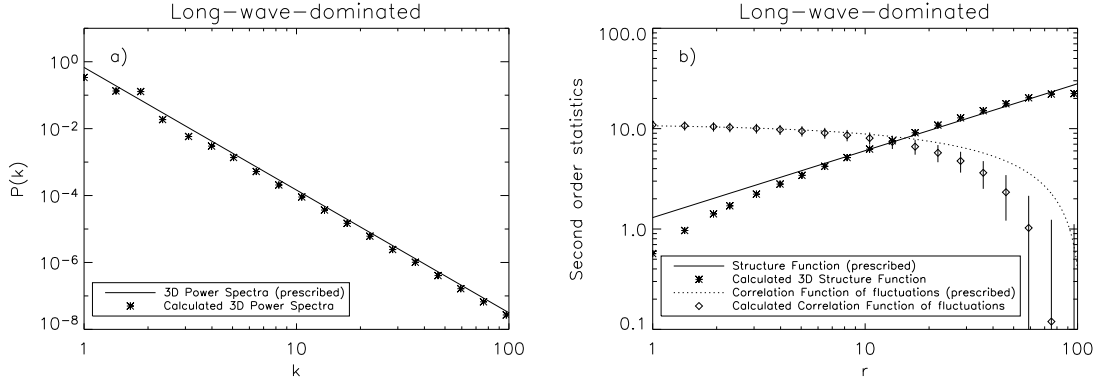


Fig. 1.— Three dimensional two point statistics of a long-wave-dominated Gaussian field (steep spectrum). In panel *a*) the three dimensional power spectrum, the solid line is the prescribed spectrum, with a spectral index of $-11/3$, the stars correspond to the calculated spectrum using FFT. In panel *b*) the expected structure function (*solid line*), the computed structure function (*stars*); the expected correlation function of fluctuations (*dotted line*), and the calculated correlation function of fluctuations(*diamonds*). The error bars plotted for the correlation functions are obtained assuming a 10% error in the determination of the variance (see discussion in text).

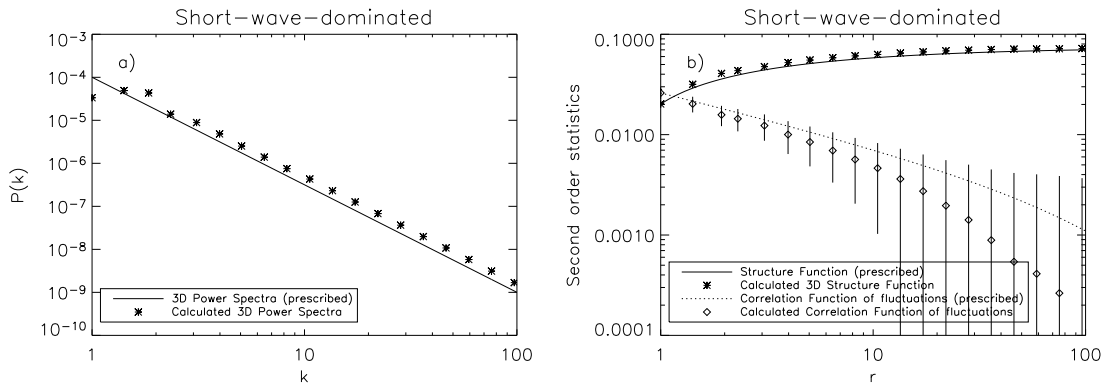


Fig. 2.— Same as Fig. 1 but for a short-dominated spectrum (3D spectral index of -2.5).

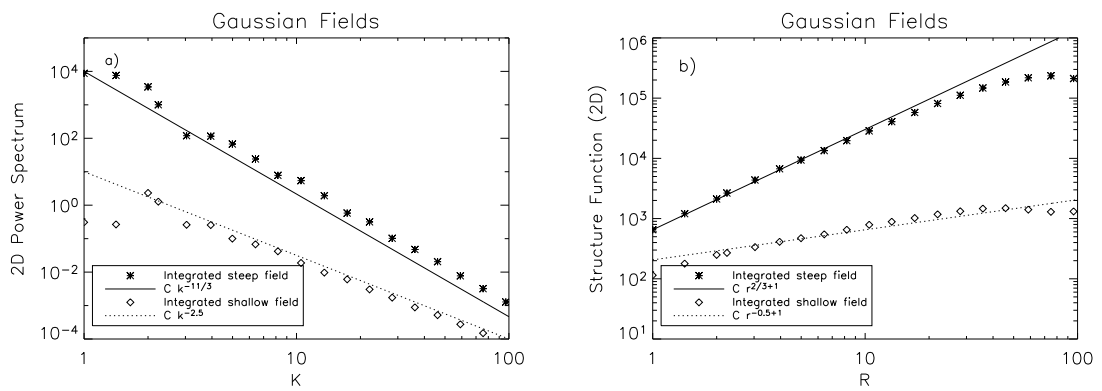


Fig. 3.— Two point statistics for Gaussian fields integrated along the z direction. In panel *a*) we show the 2D power spectra, panel *b*) correspond to the second order structure functions. The *stars* correspond to a steep spectrum with a prescribed 3D power spectrum index of $-11/3$, the *diamonds* correspond to a shallow spectrum with a prescribed 3D power spectrum index of -2.5 . In *solid* and *dotted* lines respectively, we plotted for reference the expectations for both long-wave or short-wave dominated cases. The vertical scales in panel *b*) have been modified arbitrarily for visual purposes.

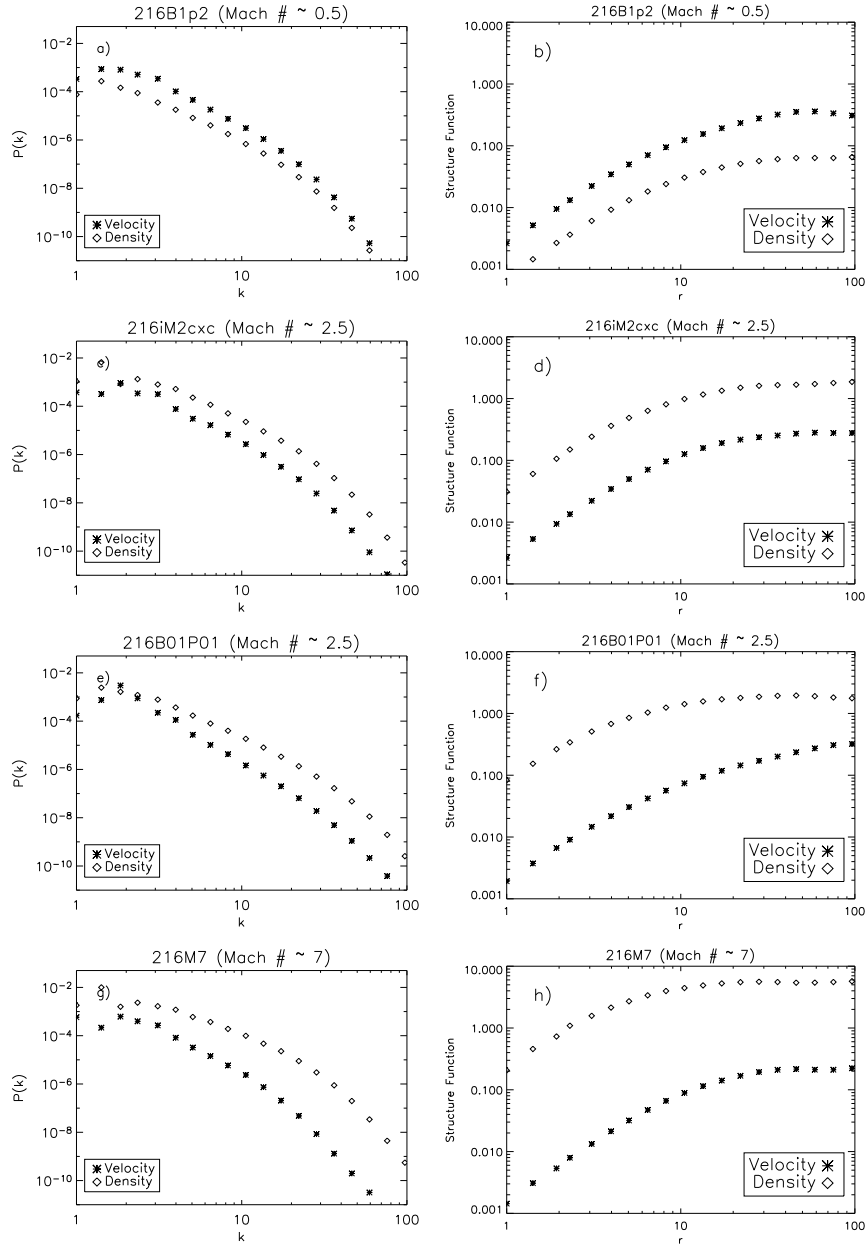


Fig. 4.— Underlying 3D statistics of the MHD simulations. On the left, the power spectra, and on the right the structure functions, the four runs are ordered in ascendant Mach number from top to bottom.

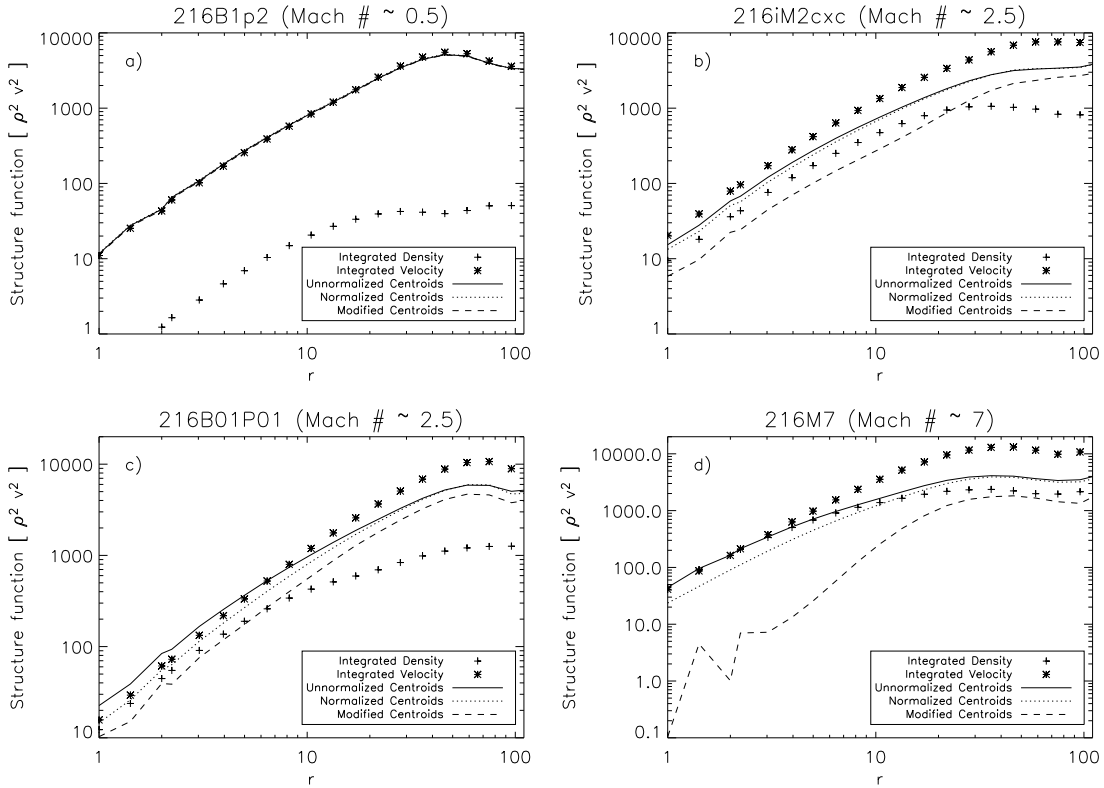


Fig. 5.— Second order structure function of the integrated density (crosses), integrated velocity (stars), unnormalized, normalized, and modified centroids (solid, dotted, and dashed lines respectively) for the four set of simulations. To allow for a direct comparison we scale the quantities to be all in units of $[\rho^2 v^2]$. (i.e. multiplied the structure function of the integrated velocity by $\langle \rho^2 \rangle$, the integrated density by $\langle v^2 \rangle$, and the normalized centroids by $\langle I^2 \rangle$). The erratic behavior of MVCs in (d) at small scales is due to numerical roundoff error.

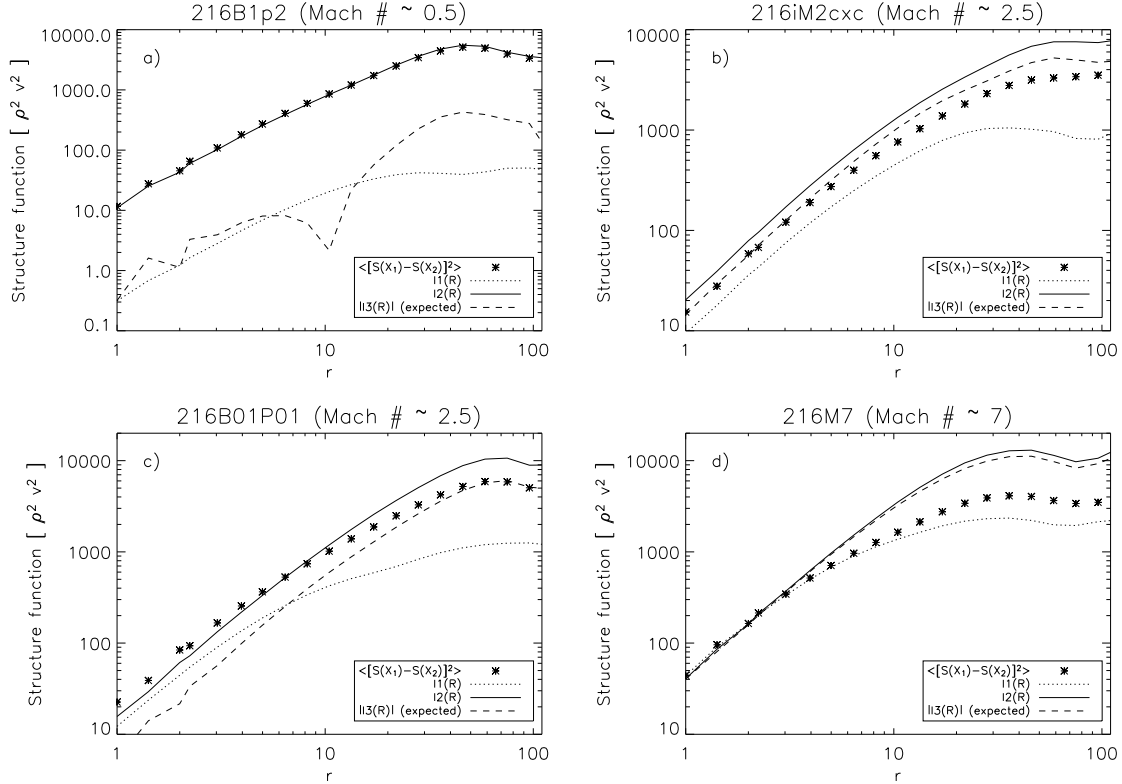


Fig. 6.— Decomposition of the structure function of the unnormalized centroids as in equations (27) and (29). The structure function of unnormalized centroids are the *stars*. The *dashed line* ($I1[\mathbf{R}]$) is the structure function of the column density (weighted by $\langle v^2 \rangle$); the *solid line* is the structure function of the velocity field integrated along the LOS (weighted by $\langle \rho^2 \rangle$), $I2[\mathbf{R}]$); the remaining terms (which include density-velocity correlations) are the *dashed line* ($I3[\mathbf{R}]$). the expected magnitude of $I3(\mathbf{R})$ is computed as $|\langle [S(\mathbf{X}_1) - S(\mathbf{X}_2)]^2 \rangle - I1(\mathbf{R}) - I2(\mathbf{R})|$

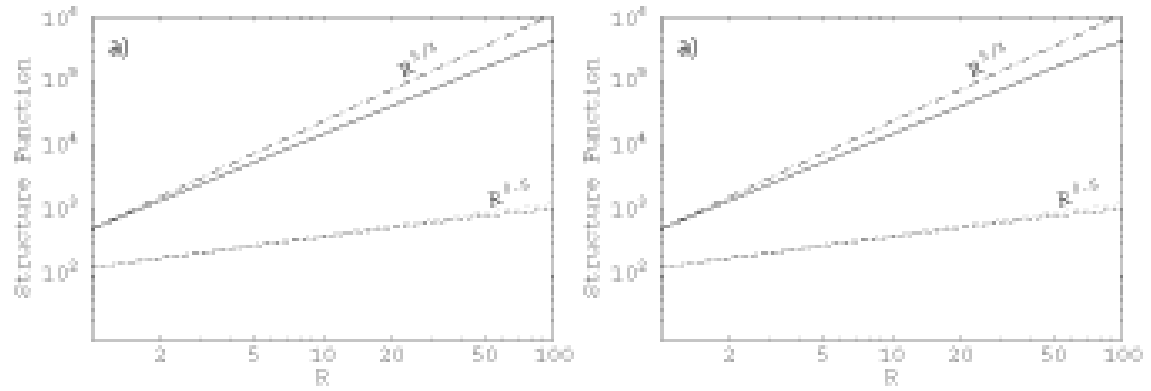


Fig. 7.— Integrated structure functions from a field with a power-law spectrum. a)The *solid* line is the exact result (numerically integrating eq.[A3]) for a field with steep spectrum (3D power spectrum index of $-11/3$), the *dashed* is line for a shallow spectrum (3D power spectrum index -2.5 , obtained numerically integrating eq.[A10]). The *dash-dotted*, are the power-law asymptotics for the steep spectrum, and the *dotted* line for the shallow spectrum. Figure b) is the same as a) but we integrated for separations beyond the thickness of the object (chosen here to be 216 to compare with the Gaussian Cubes in Figure 3), we can see clearly the effect of limited thickness discussed in the text.